Check for updates

Recent advances in hydrogel-based flexible strain sensors for harsh environment applications

Miaoyu Li,[ab] Jie Pu,[c] Qinghe Cao, [ID][c] Wenbo Zhao,[c] Yong Gao,[c] Ting Meng,[c] Jipeng Chen[c] and Cao Guan [ID] *[ac]

Flexible strain sensors are broadly investigated in electronic skins and human–machine interaction due to their light weight, high sensitivity, and wide sensing range. Hydrogels with unique three-dimensional network structures are widely used in flexible strain sensors for their exceptional flexibility and adaptability to mechanical deformation. However, hydrogels often suffer from damage, hardening, and collapse under harsh conditions, such as extreme temperatures and humidity levels, which lead to sensor performance degradation or even failure. In addition, the failure mechanism in extreme environments remains unclear. In this review, the performance degradation and failure mechanism of hydrogel flexible strain sensors under various harsh conditions are examined. Subsequently, strategies towards the environmental tolerance of hydrogel flexible strain sensors are summarized. Finally, the current challenges of hydrogel flexible strain sensors in harsh environments are discussed, along with potential directions for future development and applications.

1. Introduction

Flexible electronics technology holds revolutionary significance across various eras, including the information and artificial intelligence era.[1–3] In particular, wearable sensors converting physical stimuli into electrical signals to monitor human states and surrounding information, play a crucial role in developing the medical monitoring equipment, soft robotics, electronic skins, and human–machine interaction.[4–6] Among them, flexible strain sensors have garnered significant attention due to their high sensitivity, wide strain sensing range, and fast response time.[7–11] Unlike conventional sensors that incorporate rigid semiconductor chips and circuit boards, flexible strain sensors can be bent, twisted, stretched, and compressed while maintaining conductive paths under large and small deformations.[12,13] Furthermore, flexible strain sensors address the limitations of slow response times and non-portability associated with conventional rigid sensors. Additionally, they facilitate the detection of glucose[14] and sweat,[15] deoxyribonucleic acid (DNA) analysis,[16] *etc.*, thereby driving a technological revolution in next-generation sensors.[17,18]

[a]Institute of Flexible Electronics and Intelligent Textile, Xi'an Polytechnic University, Xi'an 710048, P. R. China

[b]School of Textile Science and Engineering, Xi'an Polytechnic University, Xi'an 710048, P. R. China

[c]Institute of Flexible Electronics, Northwestern Polytechnical University, Xi'an 710072, P. R. China. E-mail: iamcguan@nwpu.edu.cn

Miaoyu Li is pursuing her PhD degree at the Institute of Textile Science and Engineering, Xi'an Polytechnic University. She received her MS in environmental science and engineering from Xi'an Polytechnic University in 2023. Her research focuses on flexible energy storage devices.

Miaoyu Li

Jie Pu is pursuing her PhD degree at the Institute of Flexible Electronics, Northwestern Polytechnical University. She received her BS in mineral processing engineering from Chang-gan University in 2017 and her MS in materials science from Northwestern Polytechnical University in 2020. Her research focuses on multifunctional fibrous devices, including Zn-ion batteries, supercapacitors, and sensors.

Jie Pu

Currently, research on flexible strain sensors focuses on constructing efficient and stable conductive networks to produce significant responses under minor external deformations.[19] In recent years, conductive composite elastomers and metal percolation networks have been commonly used to fabricate flexible strain sensors.[20,21] However, these sensors often compromise wearing comfort due to their high mechanical stiffness. Conductive hydrogels, as a typical wet-soft material, exhibit significant potential for flexible electronics due to their biomimetic structures, favorable mechanical properties, and excellent biocompatibility.[22,23] Most conductive hydrogels are fabricated by incorporating conductive fillers (such as carbon nanotubes,[24] graphene,[25–27] polymers,[28,29] natural fibers,[30,31] and metal particles[32–34]) into cross linked non-conductive polymer matrices. The polymer matrix provides stable three-dimension support, while conductive fillers construct a conductive pathway.[35] When stretched, this pathway converts mechanical deformations into electrical signals, resulting in variations in resistance and conductivity. Therefore, by altering the conductive fillers, cross-linkers, and intermolecular interactions, the network structure, electrical properties, and mechanical properties of hydrogels can be effectively tuned over a wide range.[36,37] Furthermore, designing and optimizing a three dimensional network structure hydrogel sensor with self-healing and adhesive properties can closely conform to the skin surface, detecting subtle physiological signals and enabling real-time monitoring of human conditions.[38]

Although significant progress has been made in enhancing the performance of hydrogel-based flexible strain sensors, their practical application in extreme environments such as polar regions, deserts, and deep seas is severely limited by the water states within the hydrogel (Fig. 1). A comprehensive understanding of the challenges faced by hydrogel flexible strain sensors under harsh conditions is crucial for developing sensors capable of withstanding various extreme environmental conditions (Fig. 2). For example, at extremely low temperatures, the free water molecules within the hydrogel freeze and solidify, causing a loss of flexibility and resulting in brittle deformation, which degrades performance or leads to failure.[39] In extremely high-temperature environments, thermal expansion, deformation, and leakage of conductive fillers reduce sensing sensitivity and cause signal drift.[40] Furthermore, rapid transitions between high and low temperatures require exceptional environmental adaptability to maintain performance. Additionally, high

Qinghe Cao is currently pursuing his PhD in Prof. Guan's group at Northwestern Polytechnical University. He received his BS in materials chemistry from Shenyang University of Chemical Technology in 2016 and his MS in materials physics and chemistry from Shandong University in 2019. His research focuses on design of nanomaterials for electrocatalysis and flexible energy storage.

Qinghe Cao

Yong Gao is pursuing his PhD degree at the Institute of Flexible Electronics, Northwestern Polytechnical University. He received his BS in materials science and engineering from Fuzhou University in 2018 and his MS in materials science from Northwestern Polytechnical University in 2021. His research focuses on zinc-based batteries.

Yong Gao

Wenbo Zhao received his master's degree from Northwestern Polytechnical University in 2020. He is currently pursuing his PhD at the Institute of Flexible Electronics, Northwestern Polytechnical University. His research interests focus on metal–air batteries, flexible electronics and first-principles computing.

Wenbo Zhao

Cao Guan is a Professor and the Dean of Institute of Flexible Electronics, Northwestern Polytechnical University. He received his BS degree from School of Physics, Wuhan University, China, in 2009 and completed his PhD study in the School of Physics and Mathematics Sciences, Nanyang Technological University, Singapore, in 2013. He worked as a Research Fellow in the Department of Materials Science and Engineering, National University of Singapore, from 2014 to 2018. His research focuses on nanostructure materials for flexible electronics.

Cao Guan
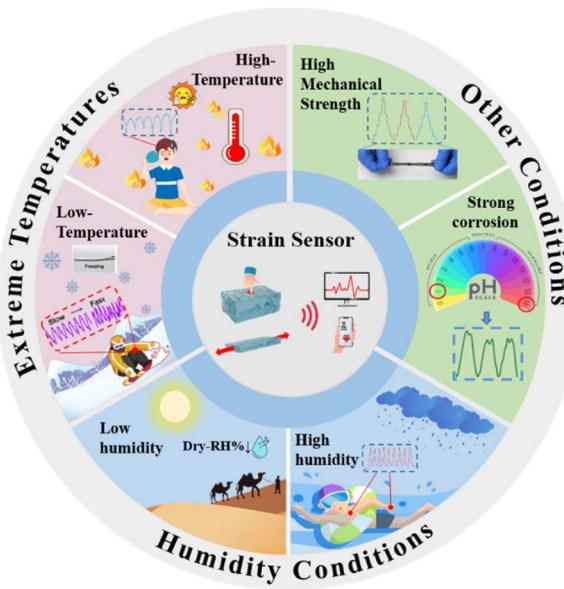
Fig. 1 Schematic overview of hydrogel-based flexible strain sensors in harsh environment applications.

humidity causes strong interactions between water molecules and hydrogen bonds, leading to swelling, short-circuiting of the conductive network, and a reduction or loss of sensing performance.[41] Conversely, in extremely dry environments, hydrogels can experience structural collapse and damage due to water

loss. Finally, extreme mechanical stress and corrosive environments can severely impact the integrity and functionality of hydrogel-based flexible strain sensors.[42–44]

This review focuses on the key challenges, current research status, and future prospects of hydrogel flexible strain sensors under harsh environmental conditions. First, we summarize the key challenges faced by these sensors in extreme environments, including freezing, water loss, swelling, cracking, and corrosion due to extreme temperatures and humidity levels. Then, we systematically discuss and review modification strategies, such as improvement of hydrogel network structure, introduction of functional additives, and interfacial modification. Finally, we propose potential perspectives to accelerate the widespread use of hydrogel-based flexible strain sensors. We hope this review will provide valuable insights for researchers looking for novel approaches to enhance the long-term stability and application of hydrogel-based flexible strain sensors under harsh conditions.

2. Extreme temperature conditions

2.1 Extremely low-temperature conditions

One principal concern for the extensive deployment of hydrogel flexible strain sensors is their temperature tolerance. In a previous study, the researchers proposed three different states of water within a flexible strain sensor hydrogel. They are free water, weakly bound water, and strongly bound water.[45] Among these, free water is the main component of the hydrogel
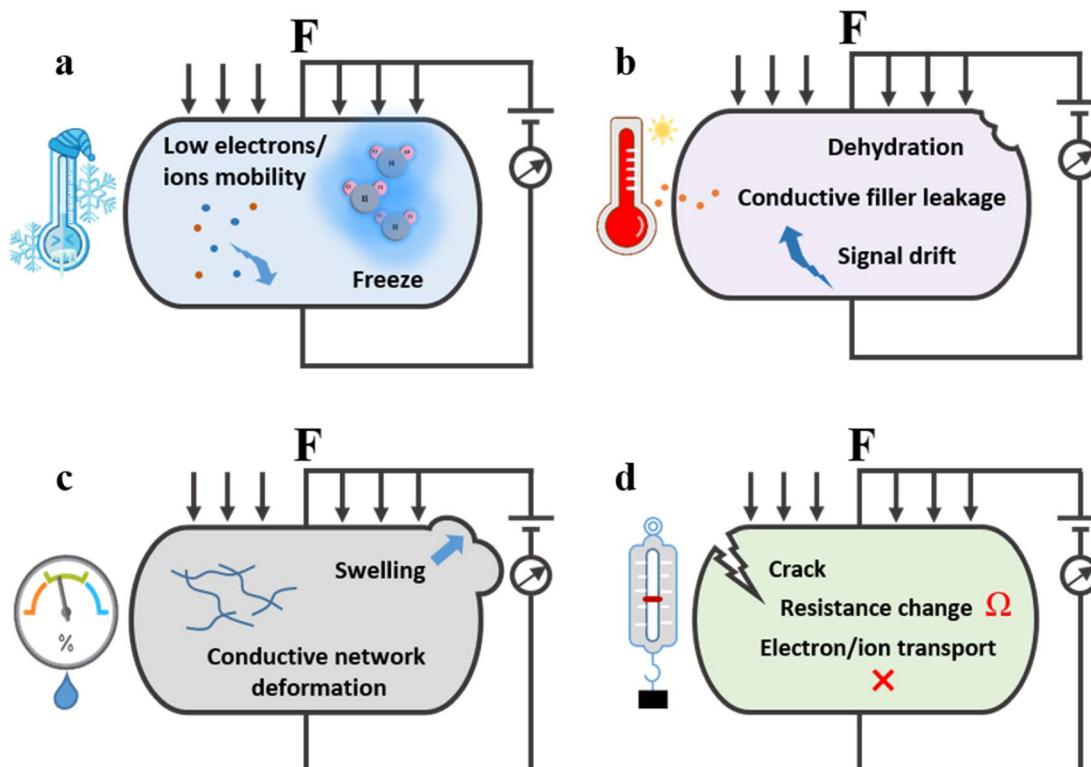
Fig. 2 Schematic illustration of the challenges faced by hydrogel flexible strain sensors under harsh conditions, including (a) low temperatures, (b) high temperatures, (c) high humidity and (d) high mechanical stretching.

network, whereas weakly bound water and strongly bound water are present in much smaller quantities. At low temperatures, free water primarily engages in hydrogen bonding and hardly interacts with the polymer network of the hydrogel. Although weakly bound and strongly bound water exhibit stronger interactions with the hydrogel network that can effectively inhibit ice crystal formation, their concentrations are too low to prevent freezing.[46] Consequently, the hydrogel network often freezes at extremely low temperatures. As the quantity of free water molecules decreases sharply, the rate of electron/ion mobility within the hydrogel network is reduced, leading to variations in resistance and slower reconstruction of reversible dynamic bonds.[47] Furthermore, the tunnelling effect is constantly weakened due to the disruption of electron/ion transport channels caused by the crystallization or phase transition of free water molecules. This leads to a reduction in the number of conductive pathways and an increase in the spacing between conduction particles, thereby causing a continuous increase in resistance and degradation of the sensing performance.[44,48–51]

To reduce or eliminate the impact of low-temperature conditions and enhance the anti-freeze performance of the hydrogel-based flexible strain sensor, various strategies have been explored. Based on previous studies, researchers have introduced soluble salts, polyol solutions, and ionic liquids into the hydrogel network. These additives stabilize hydrogel sensors at low temperatures by disrupting the hydrogen bonds between water molecules within the hydrogel network and enhancing the interactions between hydrogel networks.

2.1.1 Soluble salt modification strategies. Through introducing soluble salts, the hydrogen bonds between free water molecules in the hydrogel network are reduced and replaced by interactions between water and hydrated ions in the salt solution.[52] It can lower the freezing point by inhibiting the formation of ice crystals, ensuring the sensor is stable at low temperatures. In addition, the introduction of soluble salts can effectively enhance the electron/ion conductivity in the hydrogel conductive network.[53–55] Inspired by this, a hydrogel flexible strain sensor that exhibits excellent conductivity and outstanding anti-freezing properties has been developed by the same strategy.[56,57]

It is well-known that the Arctic and Antarctic ocean waters do not freeze at extremely low temperatures.[58] That should be attributed mainly to the strong hydration effects caused by complex media containing high concentrations of salt (NaCl) and polyionic substrates.[59,60] Inspired by this phenomenon, Wang and co-authors prepared a dual-network hydrophobic association hydrogel (PAMD–NaCl) by suit thermally initiated polymerization of sodium dodecyl sulfate (SDS), acrylamide (AM), and divinylbenzene (DVB) in saturated sodium chloride (NaCl) solution by using a one-step method (Fig. 3a).[61] The hydrogel shows excellent anti-freeze properties due to the strong hydration effect between free water and NaCl (Fig. 3b).[62,63] Furthermore, the NaCl environments inhibit hydrophobic cross-linking and improve ionic conductivity during hydrogel polymerization, resulting in soft hydrogels with excellent feature resistance, and high sensor performance

compared to a nonsaline environment at low temperatures (Fig. 3c). The hydrogels exhibit excellent flexibility, stretchability (10 200%), and desirable ion conductivity (106 mS cm^{-1}) even at extremely low temperatures. Based on their flexibility, the hydrogels exhibit high sensitivity even in tiny motions. Moreover, excellent freeze resistance can effectively reduce the impact of low-temperature freezing on the adhesion of hydrogel flexible strain sensors. Furthermore, the ionic conductivity of the hydrogel sensor was effectively improved by adding $FeCl_3$ to the hydrogel network. Meanwhile, the hydrogen bonding between water molecules inhibits the formation of ice crystals and promotes the application of hydrogel strain sensors at low temperatures.[64]

Compared to the traditional method of adding salt to the pre-gel precursor solution, the salt percolation strategy allows high concentrations of salt to penetrate into the interior of the hydrogel network through a concentration gradient and does not hinder the polymerization of the hydrogel.[65] Based on this, the hydrogel with a hybrid network structure (PAC–CGO) consists of polyacrylamide and chitosan. The incorporation of a high concentration of NaCl provides the (PAC–CGO–Na) hydrogel with strong hydration, and the Na^+ and Cl^- ions not only effectively enhanced the polymer structure and improved conductivity but also endowed hydrogel networks with excellent anti-freezing properties (Fig. 3g).[62] Compared to hydrogel networks without the introduction of NaCl, the PAC–CGO–Na hydrogel can achieve no freezing at −56.8 °C (Fig. 3d). Furthermore, sensing performance and flexibility are essential indicators of hydrogel flexible strain sensors. The PAC–CGO–Na hydrogel as a flexible strain sensor can be twisted and bent. In a low-temperature environment, it has the advantages of high sensitivity (gauge factor ∼ 6.67), fast response (≈ 120 ms), and a wide strain sensing range (0–1216%) (Fig. 3e and f). Moreover, the strain sensor also exhibited excellent stability in cyclic tensile measurements with a strain of 200%. Surprisingly, the gauge factor (GF) of hydrogel-based flexible strain sensors remains at a high retention value of over 90.0% with small or large strains.

Moreover, Wu and co-authors obtained DN hydrogels with carrageenan and polyacrylamide and soaked them in LiBr solutions. The higher content of LiBr (10–50 wt%) lowers the freezing point.[65] In contrast to the previous studies, Li^+ and Br^- tend to form a stable cluster with several free water molecules to reduce the number of hydrogen bonds to suppress ice crystallization.[66] Even at extremely low temperatures (−78.5 °C), the hydrogel retains excellent softness and sensor performance. The authors have introduced other salts (LiCl, $MgCl_2$, and KCl) that show a low freezing point, although higher than that of LiBr. These results proved the correctness of the strategy to improve the anti-freeze performance of the hydrogel by adding soluble salts. Based on the above, the hydrogel flexible strain sensors can detect a wide strain sensing range from 0.1 to 180% at low temperatures. The low limit of detection enables extremely high sensitivity at tiny stretches.

2.1.2 Polyol solvent modification strategies. With the exception of lowering the freezing point of hydrogels by the introduction of soluble salt solutions, polyol alcohol solvents
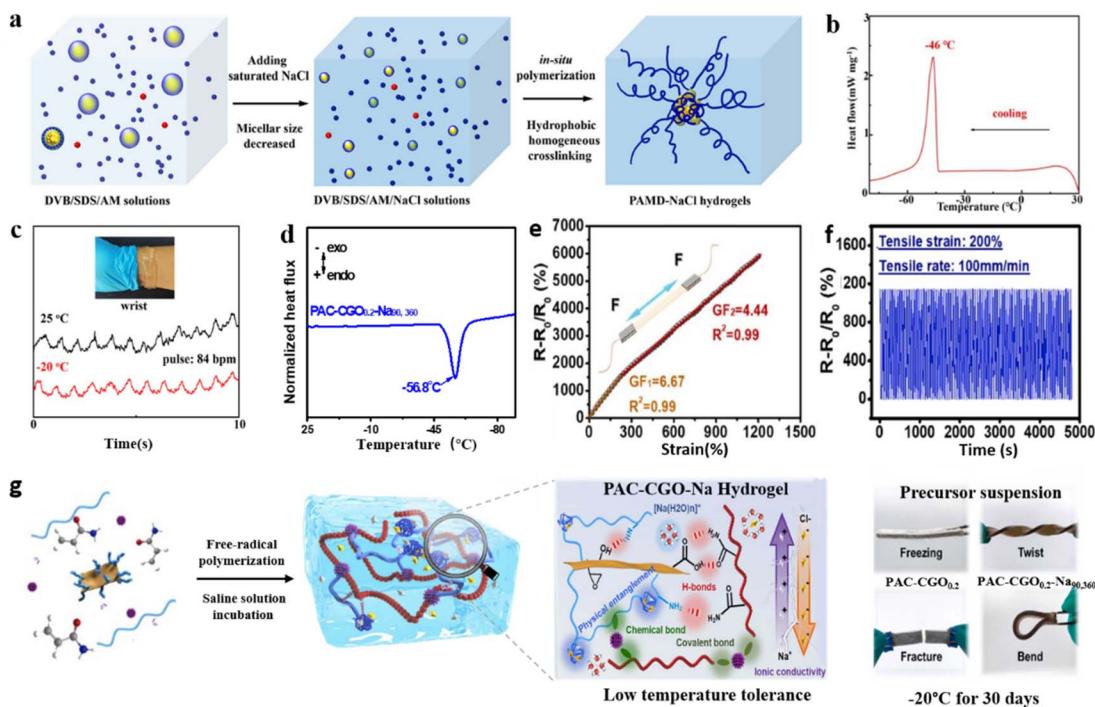
Fig. 3 Soluble salt modification strategies under extremely low temperature conditions. (a) Schematic diagram showing the manufacturing process of the salt-containing PAMD–NaCl anti-freeze hydrogel. (b) DSC trace of PAMD–NaCl hydrogels. (c) Sensing properties of the PAMD–NaCl anti-freeze hydrogel at 25 °C and −20 °C. Reproduced from ref. 61. Copyright 2023, The American Chemical Society. (d) DSC curve of the PAC−CGO$_{0.2}$−Na$_{90,360}$ hydrogel (0.2 is the weight percentage of CGO (wt%), 90 is the incubation time (min) of the hydrogel immersed in the NaCl solution, and 360 is the concentration of the NaCl solution (g L^{-1}), respectively). (e) Gauge factor of PAC−CGO$_{0.2}$−Na$_{90,360}$ hydrogels under different strains. (f) Cyclic tensile tests (200%). (g) Schematic illustration of the fabrication process of the anti-freezing PAC−CGO−Na nano-composite hydrogel. Reproduced from ref. 62. Copyright 2022, Elsevier.

have the same effect. The abundant hydrogen bonds between polyol solvents and free water molecules in the hydrogel network disrupt the formation of ice crystal lattices, thereby lowering the freezing point at low temperature.[47,67–70] At present, modification strategies involving the introduction of polyhydric solvent (*e.g.*, glycerol, ethylene glycol, *etc.*) have been successfully applied to prepare anti-freezing hydrogel flexible strain sensors by direct addition or solvent replacement.[71–73]

For example, Sun and co-authors were inspired by catechol to prepare organohydrogels (Ls–Cu@WG–PHEAA) for use as skin strain sensors. The polymerization of HEAA (*N*-hydroxyethyl acrylamide) in the glycerol–water binary phase was achieved by establishing an autocatalytic system with sodium lignosulfonate and copper(II) ions (Ls–Cu^{2+}) (Fig. 4a),[74] by controlling the ratios of water (W$_x$) to glycerol (G$_y$) to improve anti-freeze properties. By introducing non-crystallized glycerol into the hydrogel network with water as the cosolvent, the hydrogel exhibited no freezing point even at extremely low temperatures (Fig. 4b and c). Additionally, a higher content of glycerol creates a unique polyhydroxy structure that tends to form intermolecular hydrogen bonds with water molecules and the PHEAA chain, which disrupts the formation of crystal lattices of ice crystals and inhibits the growth of ice crystals. Furthermore, the increased intermolecular sacrificial bonds between Ls–Cu^{2+}–PHEAA chain glycerol form a strong physical cross-linking. This can realize effective energy dissipation

during stretching and provide outstanding tolerance to high compressive deformation.[75,76] At low temperature (−20 °C), Ls–Cu@WG–PHEAA hydrogel flexible strain sensors have relatively high sensitivity, especially at large strains. The flexible strain sensor exhibits highly sensitive sensing performance (a value of $\Delta R/R_0$ from 0 to 112%), when the different bending angles increase from 0° to 90° (Fig. 4d). With a similar strategy, Liu and co-authors proposed an interfacial engineering strategy in which tannic acid (TA, containing a high density of hydroxyl groups), encapsulated MXene to form a stable TA@MXene nanostructure.[77] They introduced TA@MXene into the poly network (hydroxyethyl acrylate) (PHEA) in glycerol/water binary solvent to obtain a hydrogel with excellent properties. The introduction of glycine (Gly) contributed to the mechanical and anti-freeze performances. The weaker hydrogen bond crosslinks with the polymer chain due to the introduction of glycerol to adapt to large strains. This inhibited the formation of ice crystals by forming hydrogen with water molecules. Even at low temperatures (−40 °C), the hydrogel used for the strain sensor exhibited large stretchability (>500%) with low hysteresis (<3%). Other researchers have similarly enabled strain sensing under extreme conditions (70 °C and −80 °C) by making hydrogels electrically conductive and mechanically stable *via* water/glycerol binary solvents.[78]

Compared to the direct-addition method, the solvent replacement method does not require consideration of the
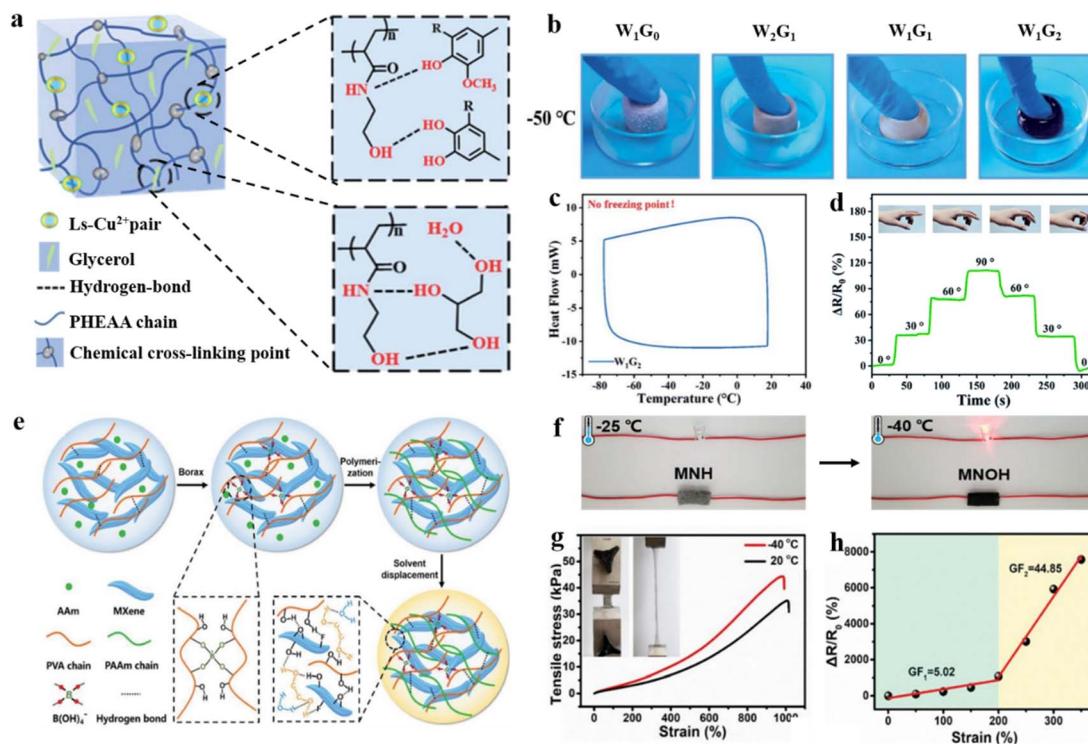
Fig. 4 Polyol solvent modification strategies under extremely low temperature conditions. (a) Schematic diagram of the water−glycerol binary phase anti-freeze organic hydrogel fabrication process. (b) The W_xG_y hydrogels at −50 °C. (c) DSC curves of the W_1G_2 hydrogel. (d) Monitoring the relative resistance variations of a finger by using an anti-freezing hydrogel strain sensor. Reproduced from ref. 74. Copyright 2021, Royal Society of Chemistry. (e) Schematic illustration of the fabrication of anti-freeze hydrogel MNOH. (f) Conductivity of MNOH and MNH at low temperature. (g) Tensile stress−strain curves of MNOH at 20 °C and −40 °C. (h) Gauge factor of MNOH hydrogels under different strains. Reproduced from ref. 67. Copyright 2019, Wiley-VCH.

impact of the added amount on the polymerization of hydrogels. The anti-freeze MXene nanocomposite hydrogel (MNOH) was prepared by immersing the MXene nanocomposite hydrogel in an ethylene glycol (EG) solution to displace a portion of the water molecules (Fig. 4e).[67] The formation of hydrogen bonds between water molecules and EG after solvent replacement inhibits the formation of ice crystal lattices and enables conductivity at low temperatures. Besides, the hydrogen bonds endowed the hydrogel with excellent stretching (≈980%, −40 °C) (Fig. 4f and g). Surprisingly, the kinetic cross-linking between PVA and tetrahydroxyboronic acid ions offers a dual effect that the supramolecular interactions between EG, PVA, and MXene provide them with excellent self-healing capabilities at sub-zero temperatures. The flexible strain sensor was prepared by using an MNOH hydrogel to monitor human activities with remarkable sensitivity (GF ∼ 44.85) and environmental tolerance over a wide strain sensing range (50–350% strain at −40 °C) (Fig. 4h).

2.1.3 Ionic liquid modification strategies. In previous studies, an ionic liquid with excellent mobility and conductivity consisting of organic cations and inorganic anions has received much attention.[79,80] Hydrogel flexible strain sensors have shown that anion–cation pairs in ionic liquids can interact with hydroxyl groups and water molecules of the hydrogel network, respectively. The interaction between the cation and the hydroxyl group is a non-covalent or π-electron interaction, and

the cation and hydroxyl hydrogen form a strong hydrogen bond. With the introduction of ionic liquids into the hydrogel sensing network, the formation of ice crystals is inhibited by the formation of hydrogen bonds with free water molecules. Meanwhile, ionic liquids composed of anions and cations can construct an ion-rich hydrogel environment, which can contribute to the improvement of ionic conductivity as well as sensing properties of the hydrogel.[81]

To widen the application of ionic liquid modification strategies in the direction of the anti-freeze hydrogel flexible strain sensor, researchers have taken several measures. Dual network hydrogels were prepared by using starch and polyvinyl alcohol (PVA). The ratio of ionic liquid ([AMim]Cl)/glycol/water ternary solvent system regulated the comprehensive performance of the hydrogels (Fig. 5a).[81] The hydrogel exhibits excellent tensile mechanical and anti-freeze properties because the $[AMim]^+$ and hydroxyl groups interact with non-covalent bonding, and strong hydrogen bonds are formed between $Cl^−$ and hydroxyl hydrogen. Due to the synergistic action of ionic liquids and EG, hydrogen bonds are formed with water molecules to prevent ice crystallization and lower the freezing point to −128.9 °C (Fig. 5b). Besides, ionic liquids create an ion-rich environment that enhances the ionic conductivity of the hydrogel at low temperature (Fig. 5c) and disrupt bacterial cell membranes through electrostatic interactions, endowing the hydrogel with
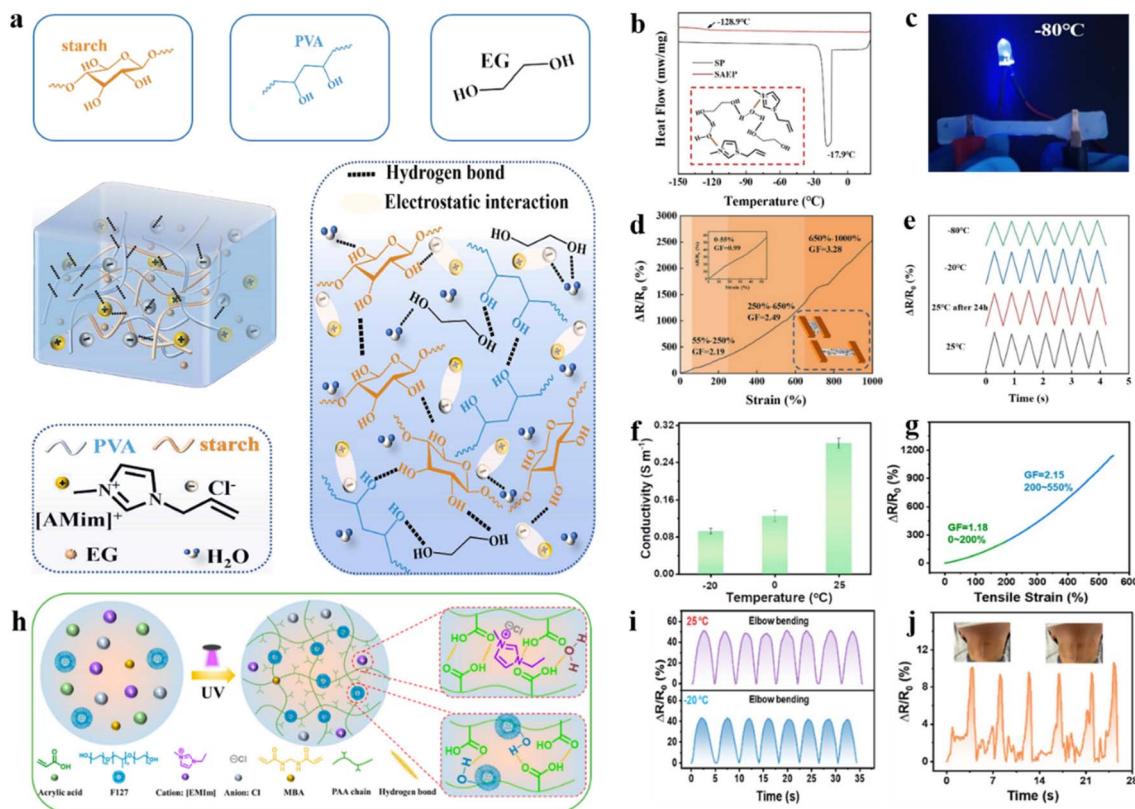
Fig. 5 Ionic liquid modification strategies under extremely low temperature conditions. (a) Schematic of the SAEP hydrogel (with starch, [AMim] Cl, EG (ethylene glycol), and (PVA) polyvinyl alcohol). (b) DSC curves of hydrogels and the anti-freeze mechanism. (c) Conductivity of the SAEP hydrogel at −80 °C (d) Relative resistance of the hydrogel under 0–1000% strain. (e) Sensing relative resistance changes of the SAEP hydrogel (at a strain of 100%) at different temperatures (25 °C, 25 °C after 24 h, −20 °C, and −80 °C). Reproduced from ref. 81. Copyright 2023, Elsevier. (f) Conductivity of the ionic hydrogel at −20, 0, and 25 °C. (g) Gauge factor of the anti-freezing ionic hydrogel strain sensor. (h) Schematic illustration of the preparation process of the ionic hydrogel. (i) Resistance signal changes to elbow bending at −20 °C and 25 °C. (j) Monitoring the relative resistance variations of swallowing using an anti-freezing hydrogel strain sensor. Reproduced from ref. 84. Copyright 2024, The American Chemical Society.

antibacterial properties.[82,83] The excellent anti-freezing properties and sensitivity of these hydrogels enable them to be used as flexible strain sensors for detecting body signals. The strain sensor demonstrates exceptional sensitivity (GF ∼ 0.99 to 3.28) across a wide strain sensing range (below 55% to 650%–1000%) (Fig. 5d). Moreover, the sensing performance is still stable at extremely low temperatures compared to room temperature (Fig. 5e). The hydrogels prepared by using an ionic liquid modification strategy exhibit excellent performance when used as flexible strain sensors due to the properties of ionic liquids. Recently, Liu and co-authors prepared a hydrogel with a binary solvent system of ionic liquid (1-ethyl-3-methylimidazolium chloride, [EMIm]Cl) and water (Fig. 5h).[84] First, the binary solvent system exhibits the electrochemical properties of an ionic liquid to ensure the ionic conductivity (0.28 S m^{-1} at 25 °C) of the hydrogel flexible strain sensor (Fig. 5f).[85] Furthermore, the hydrogen bonds between the polymer chain, water, and ionic liquid could improve the comprehensive mechanical properties of strain sensors. They exhibited excellent tensile properties (strain > 1800%), durability (1000 times at 100% strain), and satisfactory sensitivity (gauge factor ∼ 2.15 at 200% strain) (Fig. 5g). Finally, the hydrogen bonds between the ionic

liquid and water molecules hinder the formation of ice to lower the freezing point, which ensured the stability of the sensor at low temperatures (−20 °C). Furthermore, the sensor can accurately recognize small deformations such as swallowing, and has a wide application prospect (Fig. 5i and j).

2.1.4 Other modification strategies. The aforementioned reports have demonstrated both the anti-freeze properties of hydrogels and the environmental tolerance of hydrogel flexible strain sensors. Other methods can also effectively prevent freezing within the hydrogel network, enabling flexible strain sensors to operate stably in extremely low-temperature environments. For example, the anti-freezing performance of hydrogel flexible strain sensors can be further enhanced through the introduction of anti-freeze cross-linking agents.

Recently, Liu and co-authors developed a poly(hydroxyethyl-L-glycol)-based polymer cross-linker (MC) and used it to improve the properties of the hydrogel (Fig. 6a).[86] Compared to traditional short-chain cross-linkers, MC features a long chain that may change the network. When used in hydrogel based flexible strain sensors, the polar groups (hydroxyl and amide groups) in MC can form strong hydrogen bonds with water molecules, thereby lowering the freezing point.[87] An increased content of
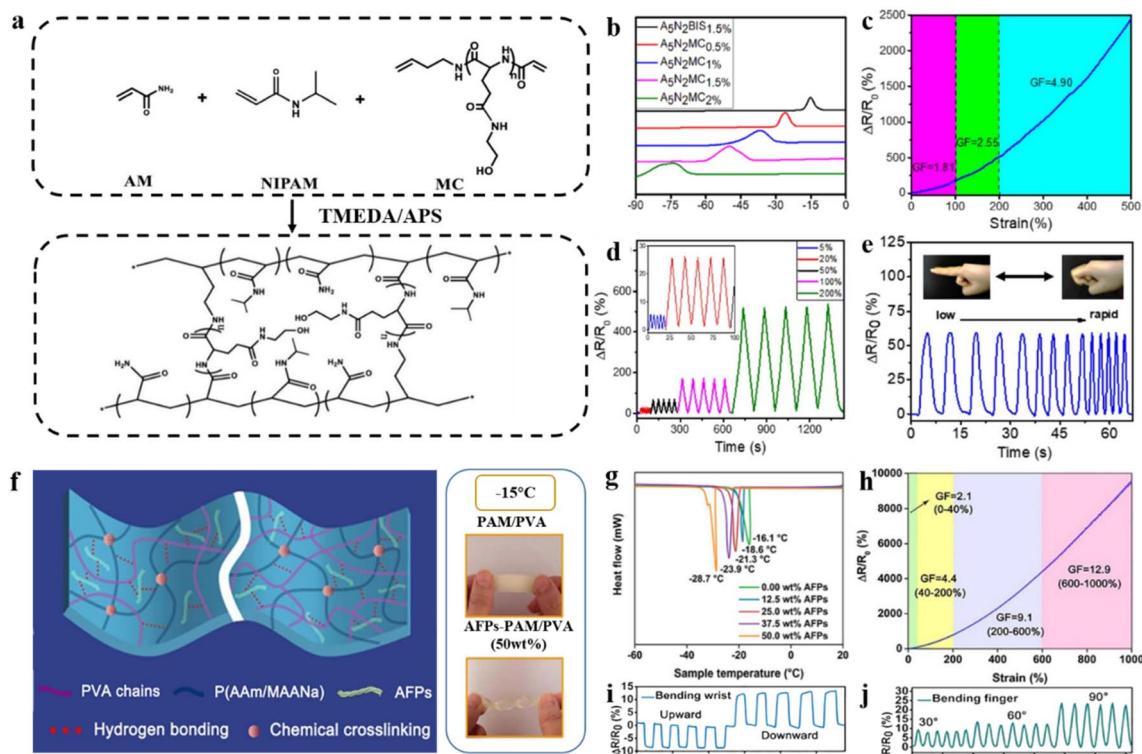
Fig. 6 Other modification strategies under extremely low temperature conditions. (a) The fabrication process of the MC cross-linked hydrogel. (b) DSC curve of anti-freeze hydrogels. (c) Gauge factor of the anti-freezing hydrogel at different strains. (d) Relative resistance change of the hydrogel during consecutive loading–unloading tests at different strains (5, 20, 50, 100, and 200%). (e) Hydrogel strain sensors are used to monitor finger binding at different speeds. Reproduced from ref. 86. Copyright 2021, The American Chemical Society. (f) Schematic illustration of the preparation process of the MC-cross-linked hydrogels. (g) DSC curves of hydrogels with different AFPs contents. (h) $\Delta R/R_0$ and GF of a hydrogel sensor over a wide range of 0–1000%. Resistance variations of the hydrogel: (i) bending the wrist and (j) bending a finger. Reproduced from ref. 88. Copyright 2021, Elsevier.

MC (0.5–2 wt%) results in a lower freezing point (−25.9 to ∼−75.9 °C) (Fig. 6b). Furthermore, the hydrogel exhibits high sensitivity (GF ∼ 1.81–2.55) in a wide range of strain (5–200%) (Fig. 6c and d). When the finger bends at the same angle with different rates, the sensor consistently obtains almost the same value for $\Delta R/R_0$, confirming its stability (Fig. 6e).

In nature, many kinds of biocompatible materials can effectively reduce hydrogel freezing points. Biocompatible anti-freeze hydrogel strain sensors were constructed by integrating natural fish anti-freeze proteins (AFPs) in a hydrogel network consisting of a chemical cross-linker (acrylamide/sodium methacrylate) and a physical cross-linker (polyvinyl alcohol) (Fig. 6f).[88] The anti-freeze proteins can adjust the ice crystallization process by selectively bonding to the surface of ice crystals and can also interact with the hydrogel network or various materials through non-covalent bonds benefiting from the multiple amino acid groups.[89,90] Overall, the ice growth prevented by AFPs provided the anti-freeze properties of hydrogel strain sensors, and the freezing point decreased with the increased content of APFs (Fig. 6g). Surprisingly, the hydrogel strain sensors with AFPs provide excellent sensitivity (GF ∼ 2.1–12.9) and fast response (0.17 s) in the field of wide strain sensing (0.3–1000%) (Fig. 6h). The advantages of low hysteresis

and high durability enable monitoring of different human movement states (Fig. 6i and j). Inspired by plants, Liu and co-authors utilized amphoteric betaine hydrochloride (BH) with hydrated lithium chloride (LiCl) to prepare an ionic co-hybrid hydrogel (PBLL), which is used as a flexible strain sensor.[91] Due to the strong hydrophilicity of BH, the strong interaction between BH and water prevents water molecules from arranging in an orderly manner at low temperatures, thus preventing the formation of ice crystals. At extremely low temperatures (−80 °C), the PBLL flexible strain sensor exhibited high conductivity (1.9 S m^{-1}) and rapid response and recovery times.

2.2 Extremely high-temperature conditions

In equatorial regions, maximum temperatures can reach 55 °C. Although some of the issues faced by hydrogel flexible strain sensors at low temperatures may be mitigated or solved at high temperatures, new problems emerge. High temperatures can alter the lattice structure and tunnelling distance, affecting the sensor's resistance and potentially causing signal shifts or instability.[50,92–94] Additionally, elevated temperature affects electron/ion mobility within the hydrogel network. The increased collision frequency of electrons and ions in the conductive network at high temperatures leads to higher

thermal kinetic energy, which in turn alters electron energy levels and affects electron transitions.[95]

2.2.1 Salt and polyol solvent and hydrogel network modification strategies. Dehydration and thermal shock present significant challenges for hydrogels at high temperatures. Using soluble salt and polyol solutions, and modifying the hydrogel networks, are effective strategies to reduce water loss. Similar to the low-temperature modification strategy, the strong hydrogen bonds formed between the polyol solvents and the water molecules inhibit the evaporation of water molecules.[96,97] Additionally, the interaction between salt and water molecules within the hydrogel network can further reduce water dissipation. Moreover, the dual-network structure of the hydrogel limits the volatilization of free water molecules, enabling the hydrogel-based flexible strain sensors to operate effectively at high temperatures.

Most recently, Li and co-authors prepared an organic hydrogel with excellent properties for flexible strain sensors by mixing cellulose nanofibers (CNFs), tannic acid (TA), polyvinyl alcohol (PVA), and NaCl in a water–glycerol (Gly) binary solvent (Fig. 7a).[98] In the hydrogel network, improved mechanical properties are attributed to the salting-out effect of NaCl on chain entanglement. Under extreme temperature conditions, the synergistic effect of sodium chloride (salt) and glycerol effectively inhibits the evaporation and freezing of water molecules within the hydrogel network. As a result, the hydrogel retains its soft and moist characteristics when twisted at high temperatures, thereby significantly enhancing its sensing performance (Fig. 7b). For practical applications, hydrogel sensors exhibit excellent electrical conductivity (0.86 S m^{-1}), strain sensitivity (GF ~ 8.54), and stability under different deformations (Fig. 7c and d). The sensor accurately detects minor/major deformations, enabling the monitoring and sensing of the human movement status, especially at extremely high temperatures (60 °C) (Fig. 7e). Slightly differently, cross-linked poly(acrylic acid-co-acrylamide) hydrogels (P(AA-co-Am)) with silica nanoparticles were prepared by photo-polymerization.[99] The hydrogel achieved excellent comprehensive performance after being immersed in calcium chloride (CaCl$_2$) solutions. This is attributed to the capability of Ca^{2+} ions to bind with water, resulting in the formation of hydrated ions that prevent the evaporation of water molecules at elevated temperatures, consequently enhancing the ionic conductivity of the hydrogel network.[100] The strain sensor exhibits low hysteresis (<7% at 400% strain), high durability, and cycle stability (10 000 cycles at 100% strain). Additionally, the sensor exhibits a remarkable ability to precisely recognize and categorize 15 sign language gestures, thereby enabling their integration and utilization within the advanced domain of human–computer interaction technologies. A dual-network organohydrogel was prepared based on hyaluronic acid and polyacrylic acid–acrylamide for multifunctional strain sensors by introducing glycerol into the organohydrogel network via a solvent substitution strategy.[101] Due to the water-locking effect of glycerol and the
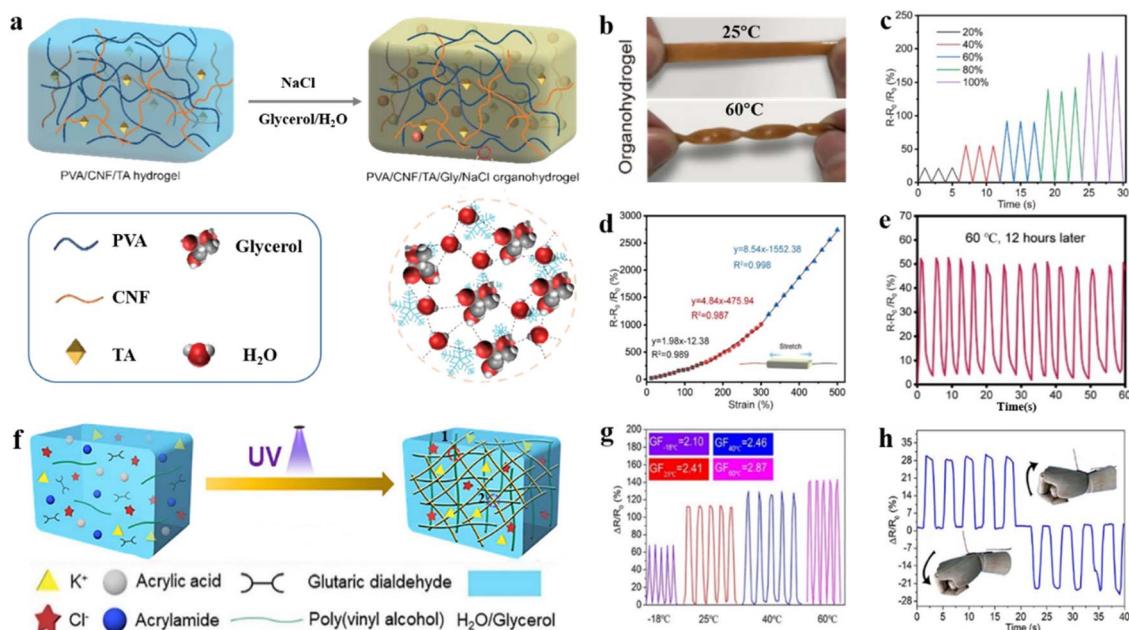

Fig. 7 Salt and polyol solvent and hydrogel network modification strategies under extremely high temperature conditions. (a) Schematic illustration of the fabrication process of the PVA/CNF/TA/Gly/NaCl hydrogels. (b) Organic-hydrogels in different environments (24 h). (c) Relative resistance of the sensor at different tensile strains. (d) Relative resistance changes at different strains. (e) Monitoring the relative resistance changes of finger movement signals after 12 h at 60 °C. Reproduced from ref. 98. Copyright 2022, Springer. (f) Schematic diagram of the DN organic hydrogels. (g) Resistance changes of the hydrogel of the flexible strain sensor under 100% strain at different temperatures (−18 °C, 25 °C, 40 °C, and 80 °C). (h) Resistance changes in the hydrogel during cyclic stretch-flexion of the wrist joint. Reproduced from ref. 102. Copyright 2021, Elsevier.

tough polymer backbone, the resulting organohydrogel exhibits stable stretchability and temperature tolerance, enabling stable operation over the range of −30 to 60 °C. In addition, it has excellent flexibility and stable electrical conductivity.

Apart from the established methods, stable operation of hydrogel flexible strain sensors at high temperatures can also be achieved *via* dual-network (DN) hydrogel construction. A binary solvent of potassium chloride and glycerol–water was introduced into the DN hydrogels polymerized using glutaraldehyde cross-linked polyvinyl alcohol (PVA–GA) and poly(acrylic acid-*co*-acrylamide) (P(AA-*co*-Am)) (Fig. 7f).[102] During the cross-linking process of the dual network, glycerol easily forms hydrogen bonds with the polymer chains, thereby inducing physical cross-linking.[103] Glycerol can form hydrogen bonds with water molecules, effectively inhibiting the evaporation of water molecules at high temperatures.[104] Furthermore, the interactions between physical and chemical cross-linking in DN networks exhibit a stabilized storage modulus (G') across a wide range of temperatures (from −20 °C to 100 °C). The flexible strain sensor utilizing the DN hydrogel has outstanding temperature tolerance (from −18 to 80 °C), high stretchability (>2000%), stability (in different temperature environments), and sensitivity, making it ideal for applications in monitoring human motions. Stable sensing performance and high sensitivity enable accurate feedback on movements such as wrist bending, thereby contributing to the widespread application of sensors under high-temperature conditions (Fig. 7g and h).

2.2.2 Other modification strategies. Complete surface exposure and weak interactions within hydrogel networks primarily contribute to water loss at high temperatures. Due to

the lack of interaction between the free water molecules and the polymers in the hydrogel network, the water molecules are released into the environment unprotected at high temperatures.

From this perspective, the coating strategy effectively prevents direct exposure of the hydrogel to air and mitigates the rate of moisture loss. Lu and co-authors prepared a multilayer structured flexible strain sensor with an inner layer of ionic hydrogel (S-PAM). This layer was composed of a semi-interpenetrating network created with sodium carboxymethyl cellulose (CMC), lithium chloride (LiCl), and polyacrylamide (PAM) (Fig. 8a). In the inner layer of the hydrogel network, strong bonds between water molecules and Li^+ and Cl^- ions are difficult to disrupt, effectively inhibiting water evaporation at elevated temperatures. The outer layer was fully encapsulated with polydimethylsiloxane (PDMS).[105] The sialon groups on the silane coupling agent condense between the inner hydrogel and the outer elastomer to form a siloxane bond. This bond enhances the adhesion between the inner and outer interfaces while also providing the sensors with excellent mechanical properties and water retention at high temperatures. The strain sensors constructed from a hybrid of hydrogels and elastomers demonstrate high sensitivity (gauge factor ∼ 3.8) over a wide temperature range (−20 °C to 60 °C) (Fig. 8b and c). Similarly, an encapsulated hydrogel with superior water retention properties was developed through a double-layer hydrophobic coating. This coating incorporates (3-aminopropyl)triethoxysilane as a chemical binder, thereby facilitating the stable operation of hydrogel strain sensors at elevated temperatures.[106]

In addition to the aforementioned modification strategies, doping can effectively alter the internal network structure of the
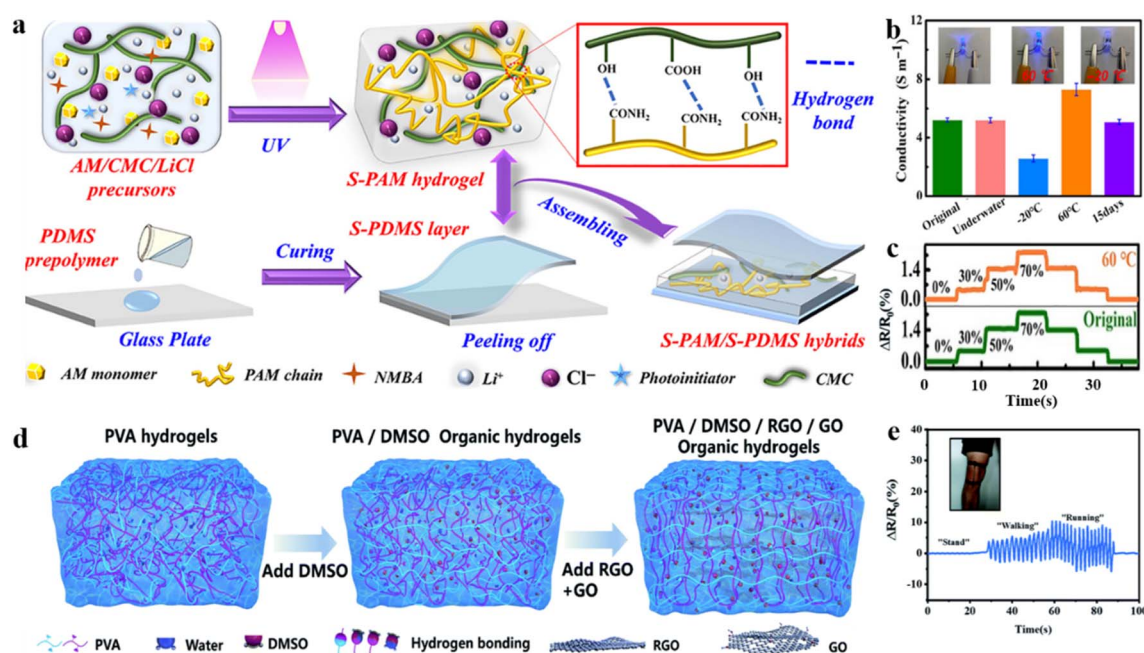

Fig. 8 Other modification strategies under extremely high temperature conditions. (a) Preparation of hydrogel–elastomer (S-PAM/S-PDMS) hybrids. (b) Conductivities of the hybrids in various environments. (c) Cycling stability tests of $\Delta R/R_0$ in different environments. Reproduced from ref. 105. Copyright 2022, Wiley-VCH. (d) Schematic illustration of the preparation process of the PDGR (PVA/DMSO/RGO/GO) hydrogel. (e) Monitoring the relative resistance changes of leg movement. Reproduced from ref. 107. Copyright 2021, Royal Society of Chemistry.

hydrogel, thereby enhancing its temperature tolerance. Reduced graphene oxide (RGO) and graphene oxide (GO) nanosheets were incorporated into porous, physically cross-linked polyvinyl alcohol (PVA) hydrogel networks using a dimethyl sulfoxide (DMSO)/water binary solvent system (Fig. 8d).[107] The interaction of DMSO with polymer chains in the hydrogel network and the strong interaction between GO and PVA chains established a more intact hydrogel network to confer long-term environmental stability. The honeycomb-like micro-network structure and the uniformly dispersed conductive fillers (GO/RGO), which are rich in functional groups, confer the hydrogel network with exceptional stretchability (3.1 MPa at 600% strain) and excellent conductivity. Hydrogels as multifunctional sensors exhibit excellent sensitivity in a wide temperature range (from −30 °C to 60 °C) to monitor physiological signals (Fig. 8e).

3. Extreme humidity conditions

3.1 Extremely high humidity conditions

In high humidity areas, the hydrophilic groups of the polymer in the hydrogel network absorb water from the environment and swell. Swelling phenomena compromise the integrity of the network structure, degrade mechanical properties, and lead to distortion or interruption of sensor signals.[108–112] Moreover, a concentration gradient develops between the conductive network of the hydrogel sensor and the high-humidity environment. In a high humidity environment, the electrons/ions in the hydrogel network can leak by diffusion across the interface, which leads to short-circuiting of the conductive network in the sensor.[113,114]

3.1.1 Hydrophobic network modification strategies. By introducing hydrophobic chains and grafting hydrophobic groups onto the hydrophilic backbone, hydrophobic networks are formed through electrostatic synergy facilitated by hydrophobic interactions.[113,115] By this means, the interfacial migration of water molecules between the internal network of hydrogel flexible strain sensors and the external high humidity environment can be effectively blocked. Consequently, it enhances the swelling resistance and mechanical properties of the hydrogel under high humidity conditions.[116]

For example, hydrogels with a dense hydrophobic network structure were developed through hydrophobic and electrostatic interactions between the cationic surfactant N-hexadecyltrimethylammonium chloride (CTAC) and poly(acrylate-methacrylate octadecyl ester) [P(AA–SMA)], as well as double cross-linking and incorporation of CMC–Na (Fig. 9a).[116] In the hydrogel network, the hydrophobic long-chain alkyl groups in CTAC interact electrostatically with the –COO groups on the P(AA–SMA) chain, serving as cross-linking points that effectively enhance the anti-swelling properties.[117,118] Additionally, the hydrophobic SMA was grafted onto the hydrophilic PAA chain to form a double cross-linked network, thereby increasing the cross-link density and enhancing resistance to swelling. Notably, the mechanical properties remained exceptional after immersion in water for 7 days (Fig. 9b). Furthermore, the hydrogel exhibited outstanding anti-swelling properties across

various liquid environments (Fig. 9c). The hydrogel was fabricated into flexible strain sensors that exhibit high sensitivity in the wide range of 0–400% (GF ∼ 1.55–5.03). Moreover, hydrophobic interfaces can disrupt the hydrated layer on the surface of hydrogels, facilitating the formation of strong connections between the target interfaces. Thus, hydrogels are well-suited for real-time underwater sensing applications (Fig. 9d and e). Similarly, based on the principle that myristyl methacrylate forms hydrophobic chain segments through electrostatic interactions within cetyltrimethylammonium bromide micelles, Du and co-authors fabricated hydrogels exhibiting enhanced anti-swelling properties (Fig. 9f).[119] Additionally, the entanglement of chitosan chains within the hydrogel network, combined with electrostatic interactions, endows excellent anti-swelling and mechanical properties to the hydrogels by forming robust hydrogen bonds with phytic acid. In hydrogel networks, hydrophilic-hydrophobic copolymers with non-uniform hydrophobic structures can locally adsorb water. Meanwhile, dynamic hydrophobic association (HA) induced by electrostatic interactions can effectively modulate the hydrophobic structural domains, thereby inhibiting water penetration.[120] The hydrogel exhibited negligible swelling after 15 days of immersion in water (Fig. 9g). The well-ordered hydrophobic structure, achieved through electrostatic interactions, afforded hydrogel high elongation (1500%) and exceptional elastic recovery behavior (elastic recovery up to 95%). Underwater, the hydrogel-based flexible strain sensors exhibit excellent sensitivity (gauge factor ∼ 1.45) over a strain range of 0–500% (Fig. 9h and i). These sensors, prepared from the hydrogel, are employed for monitoring human signals. The distinct step signals corresponding to finger bending, as illustrated in Fig. 9j, enable practical applications in underwater signaling and sensing.

Hydrogels with fully hydrophobic structures can be achieved for flexible strain sensing by polymerizing hydrophobic monomers (tert-butyl acrylate, t-BuA) within hydrophobic ionic liquids (1-butyl-3-methylimidazolium bis(trifluoromethane sulfonyl)imide, [BMIm]TFSI).[121] In liquid environments, a dense hydrophobic interface is formed by the aggregation of hydrophobic polymers within the hydrogel network. This structure effectively blocks the cross-interface diffusion of water molecules, thereby realizing the anti-swelling function of ionic liquid gels. Consequently, these hydrogels enhance the range of applications for flexible strain sensors, particularly for high-humidity sensing.

3.1.2 Other modification strategies. In order to improve the stability of hydrogel-based sensors working in high humidity environments, the cross-linking density of the hydrogel can be increased by incorporating additional cross-linking interactions. In addition, the cross-linking density and underwater stability of hydrogels are similarly improved through other interactions, such as metal coordination, chain entanglement, and the formation of microcrystalline domains. These strategies enable the stable operation of hydrogel-based flexible strain sensors in high-humidity or water environments.

To resist the swelling behavior of hydrogels used as flexible strain sensors in high humidity environments, Sun and co-authors developed an excellent anti-swelling hydrogel (PAM–
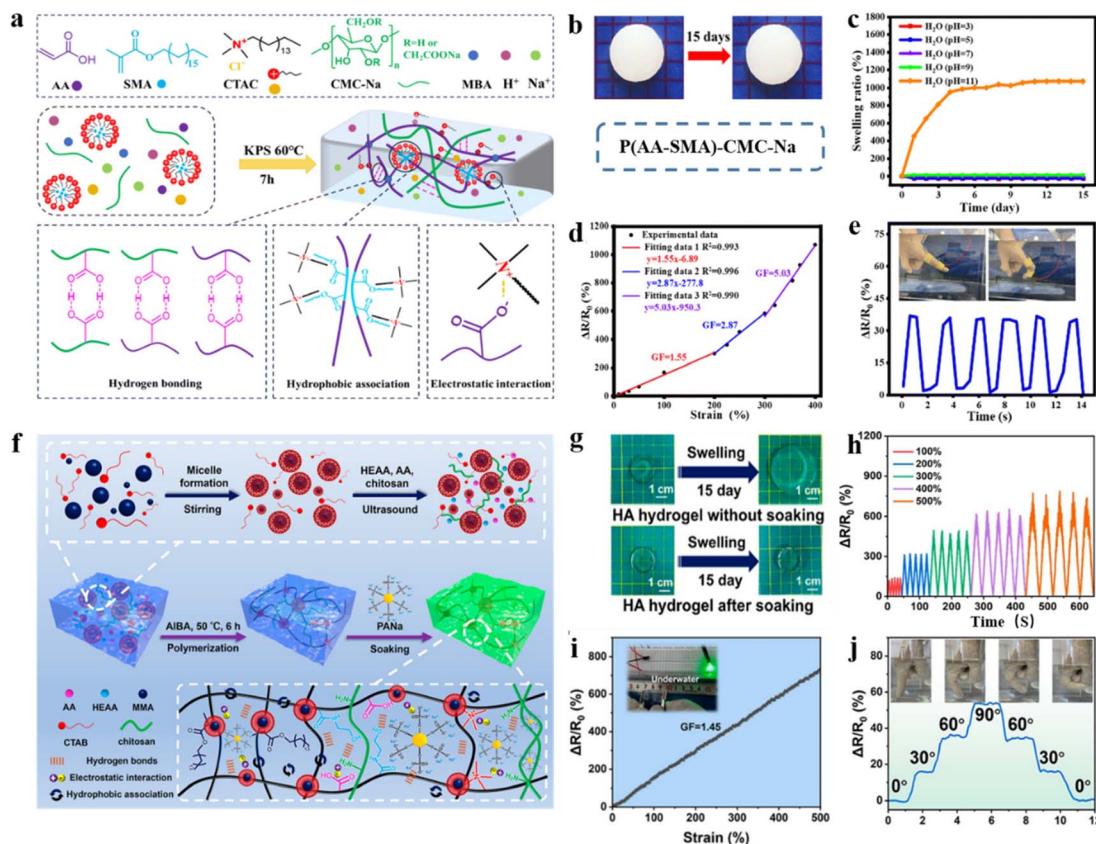
Fig. 9 Hydrophobic network modification strategies under extremely high humidity conditions. (a) Preparation of the anti-swelling P(AA−SMA)−CMC−Na hydrogel. (b) Image of the P(AA−SMA)−CMC−Na hydrogel after 15 days of immersion in water. (c) Swelling curves of hydrogels immersed in water (pH = 3, 5, 7, 9, 11) for 15 days. (d) Relative resistance variation ($\Delta R/R_0$) of the P(AA−SMA)−CMC−Na hydrogel at 0−400% strain and the homologous gauge factor (GF). (e) Relative resistance changes for finger bending in seawater. Reproduced from ref. 116. Copyright 2023, Royal Society of Chemistry. (f) Schematic of the preparation process of constructing multiple physically (hydrogen bonds, electrostatic interaction, hydrophobic association) interacted HA hydrogels. (g) Swelling behavior of hydrogels immersed in water for 15 days. (h) Relative resistance changes under different strains (100−500%). (i) Sensing properties of the hydrogel-based strain sensor underwater. (j) Monitoring the relative resistance changes of finger bending underwater. Reproduced from ref. 119. Copyright 2024, The American Chemical Society.
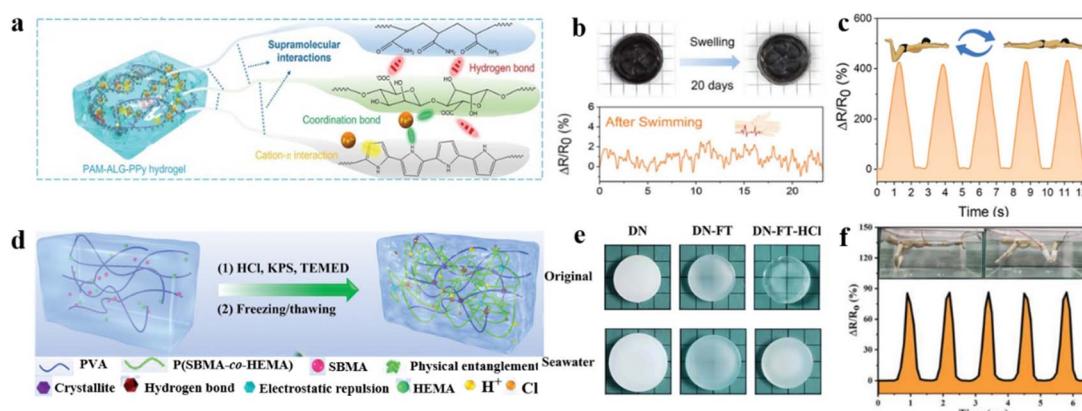
Fig. 10 Other modification strategies under extremely high humidity conditions. (a) Interactions between polymer networks in PAM−ALG−PPy. (b) Images of the PAM−ALG−PPy hydrogel after immersion in water for 20 days. (c) Monitoring the relative resistance changes of underwater motion. Reproduced from ref. 122. Copyright 2023, Wiley-VCH. (d) Schematic illustration of the fabrication process of the DN−FT−HCl (hydrogels obtained by HCl treatment after freeze/thaw treatment of copolymers consisting of PVA, SBMA and HEMA) hydrogel. (e) Swelling behavior of hydrogels immersed in seawater. (f) Relative resistance changes of DN−FT−HCl hydrogel sensors for underwater motion detection. Reproduced from ref. 123. Copyright 2022, Wiley-VCH.

ALG–PPy) by incorporating hydrogen, coordination bonds, and cation–π interactions (Fig. 10a).[122] The multi-network hydrogel was synthesized *via* a two-step polymerization process, comprising the free radical polymerization of a pristine solution of acrylamide (AM) and sodium alginate (ALG), followed by the *in situ* polymerization of pyrrole (Py) within the hydrogel network. Hydrogels with significant tensile strength properties (1.63 MPa) and elongation at break (453%) were synthesized using a supramolecular strategy. As a flexible strain sensor, the hydrogel exhibits high conductivity (2.16 S m^{-1}), a wide strain sensing range (0–400%), and exceptional sensitivity (gauge factor ∼ 4.1). The flexible strain sensors exhibit outstanding resistance to swelling, with the hydrogels maintaining virtually unchanged dimensions after 20 days of immersion in deionized water and seawater. These properties enable the sensor to facilitate real-time monitoring of underwater motion and communication (Fig. 10b and c).

In addition to exploiting the metal ion coordination within the hydrogel network to achieve anti-swelling properties, an anti-swelling hydrogel flexible strain sensor was fabricated by polymerizing [2-(methacryloyloxy)ethyl]dimethyl-(3-sulfopropyl)ammonium hydroxide (SBMA) and 2-hydroxyethyl methacrylate (HEMA) copolymer networks into polyvinyl alcohol (PVA) microcrystalline domains (Fig. 10d).[123] The formation of PVA microcrystalline domains was promoted by a freezing/thawing treatment, which provided cross-linking bonds for the amorphous hydrogel network, thereby enhancing the mechanical strength of the hydrogel.[124] The incorporation of the amphiphilic ion SBMA creates ion migration channels that facilitate bulk ion transport, enhancing conductivity. Specifically, hydrochloric acid protonates the negatively charged SO_3^- groups in SBMA, resulting in electrostatic repulsion between cations and the elimination of water molecules. This reduction in osmotic pressure improves the anti-swelling properties of the hydrogel. As an underwater strain sensor, the hydrogel exhibits negligible swelling even when immersed in water or seawater. The sensitivity (gauge factors ∼ 1.434, 2.448, and 3.356) remains satisfactory over a wide strain sensing range (0–100%, 100–200%, and 200–300%), even during immersion in water or seawater (Fig. 10e). Moreover, when subjected to loading and unloading, the sensor exhibits notably short response (130 ms) and recovery times (200 ms).

After 1000 cycles under 50% strain, the hydrogel sensor exhibited zero degradation. Based on the above properties, the sensor is used to recognize different ranges of strain, including head raising, arm swinging, and finger bending, facilitating real-time motion monitoring in underwater environments (Fig. 10f).

3.2 Extremely dry conditions

The water molecules can easily evaporate from the hydrogel network under extremely dry conditions. The hydrogel network does not retain enough strongly bound water to sustain its wet-soft properties, resulting in diminished flexibility of the strain sensor.[125–128] Furthermore, the evaporation of water molecules

results in a depletion of charge carriers within the hydrogel network[129,130] The deterioration in the conductivity of the hydrogel network leads to a subsequent degradation in sensing performance.

In order to solve the above problems, the content of free water in the hydrogel network can be reduced or locked. An anti-drying hydrogel (SPGLH) was developed by using the synergistic water retention effect of glycerol and lithium chloride (Fig. 11a).[131] In the hydrogel network, Li$^+$ ions formed hydrated complexes, while glycerol established hydrogen bonds with water molecules, resulting in physical entanglement of the polymer.[97,132–134] In addition, the introduction of LiCl contributed to the conductivity of SPGLH (Fig. 11b). Compared to the unmodified hydrogel sensors, the SPGLH sensor retained stretchability and adhesion due to excellent anti-drying properties when left at 22 °C/11% RH for 1 h (Fig. 11c). It can operate continuously for 40 hours at 20% relative humidity and maintains stable sensing capability at different humidity levels (10–70% RH) as a flexible strain sensor. Flexible strain sensors are capable of monitoring daily human body movements and enabling human–computer interactions to address real-time sensing requirements. Similarly, the hydrogels with anti-swelling properties were synthesized by homogeneously dispersing the nanofillers TA@HAP NWS, AlCl$_3$, and PVA in a binary solvent of ethylene glycol (EG) and water (W).[135] The binary system of EG and water mitigates the evaporation of water in dry environments. The fabrication of flexible strain sensors with a wide linear sensing range (350%) and high sensitivity (GF ∼ 2.84) by using hydrogels is an essential contribution to the future of multifunctional ionic hydrogel sensors.

Furthermore, coatings as protection layers on the hydrogel surface can prevent water evaporation from the hydrogel network, thereby physically mitigating water loss and enhancing water retention properties.[136] The hydrophobic hydrogels (C-PAM) were fabricated by coating the surface of micelle-crosslinked polyacrylamide (PAM) hydrogels with a poly(butyl acrylate) emulsion (Fig. 11d).[137] The coatings formed a dense hydrophobic layer on the surface of the hydrogel, which largely hindered the diffusion of water molecules in the porous structure of the hydrogel (Fig. 11e).[138,139] Excellent anti-drying properties are evidenced by a weight retention of 84 ± 0.45% even after 7 days at room temperature. A highly stable $\Delta R/R_0$ was observed at 100% tensile strain before drying and after 7 days of drying under 100 cycles of continuous cyclic loading, which shows the potential for long-term applications (Fig. 11f). Surprisingly, the dynamic micellar cross-linking in hydrogel networks provided an extremely high working range (elongation at break over 5000%). In practical applications, the sensor exhibits high application potential with the advantages of rapid, accurate, and repeatable detection of human motion.

4. Other extreme conditions

4.1 Extreme mechanical strength conditions

One principal factor for the extensive deployment of hydrogel flexible strain sensors is their mechanical strength. High
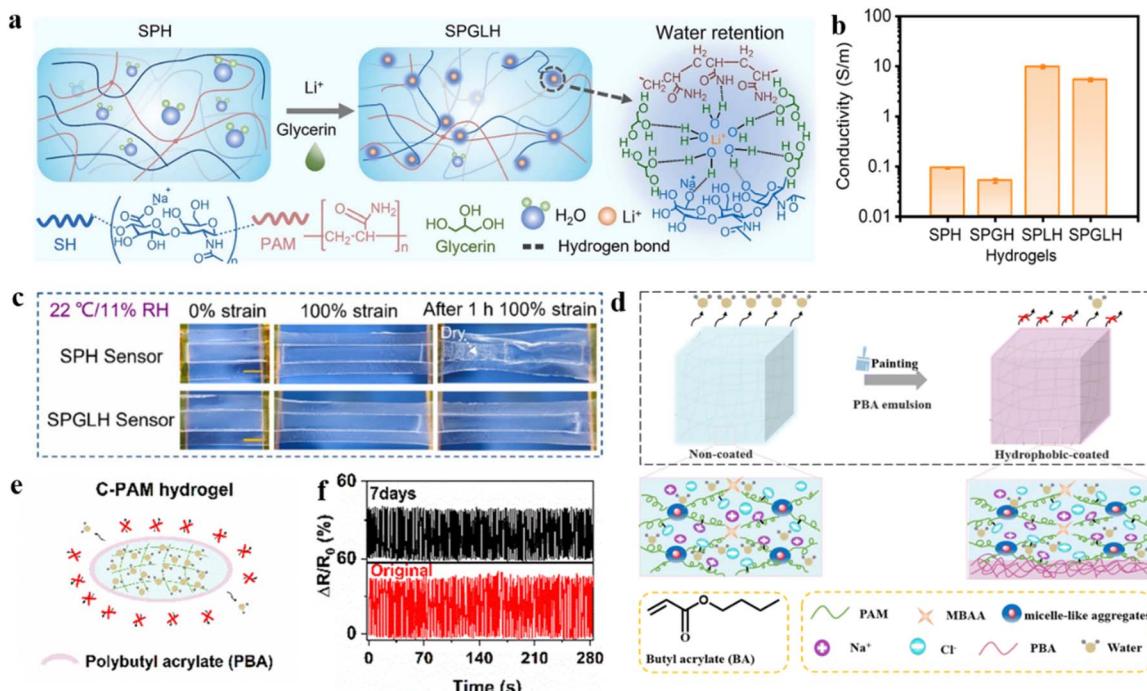
Fig. 11 Modification strategies under extremely dry conditions. (a) Preparation of hydrogels with water retention properties. (b) The conductivity of SPH, SPGH, SPLH, and SPGLH hydrogels. (c) Water-retention properties of the SPH and SPGLH sensors under 22 °C/11% RH. Reproduced from ref. 131. Copyright 2023, Elsevier. (d) Preparation of C-PAM hydrogels with core–shell structures. (e) Schematic diagram of the anti-drying hydrogel. (f) Cyclic tensile test of the C-PAM hydrogel at 100% strain before and after 7 days of storage under ambient conditions. Reproduced from ref. 137. Copyright 2023, Royal Society of Chemistry.

mechanical stress can cause deformation and cracking of the flexible substrate of the sensor, as well as insufficient bonding at the interface between the flexible substrate and the conductive material, leading to slippage.[140,141] Under high mechanical stretch conditions, hydrogel strain sensors suffer from hysteresis due to the irreversible energy dissipation of viscoelastic elastomers.[142,143] The resistance change dominated by the tunnelling effect leads to a signal drift hysteresis. As the tensile strain increases, the conductive particles become more widely separated, thereby reducing the number of effective conductive pathways and ultimately leading to sensor failure.[144] In addition, continuous loading–unloading of the stresses applied to the flexible strain sensors and cracks along the perpendicular direction of stretching lead to irreversible cracking of the interconnections between the conductive lamellae, which results in a complete disruption of the conductive pathway.[145,146]

4.1.1 DN hydrogel modification strategies. DN (dual network) hydrogels exhibit higher toughness and strength compared to traditional single network hydrogels. DN hydrogels can effectively transfer stress and dissipate capacity within their network. Typically, the first network is rigid, tough, and strong, comprising long chains with high covalent cross-linking, while the second network is soft and flexible, consisting of short chains with physical cross-links.[147,148] Such structures are able to reduce the effect of mechanical stress on the sensing performance of hydrogels by internal network synergies during external stress.

Most recently, a dual-network hydrogel was constructed by introducing a rigid cellulose/Zn^{2+}/Ca^{2+} network into a flexible polyvinyl alcohol (PVA)/borax network (Fig. 12a).[149] Among them, PVA/borax hydrogels are synthesized by the formation of dynamic borate bonds between borate ions and two diol units, which have high stretchability.[150–152] The entanglement of flexible and rigid networks is achieved by adjusting the cross-link density of the hydrogel network. The interaction between the rigid and flexible networks generates an additional energy dissipation mechanism to improve the stretching resistance of the hydrogel further (Fig. 12b).[153,154] Furthermore, the coordination of metal ions with tetrahedral borate ions, $B(OH)_4^-$, provides the hydrogel with conductivity.[155] The hydrogel was assembled as a strain sensor, and demonstrates high sensor sensitivity (GF ∼ 0.7–1.04) over a wide strain sensing range (0–600%) and stability under multiple tensile cycling conditions (Fig. 12d). Moreover, it demonstrated a reasonable corresponding response time (124 ms) and recovery time (187 ms) during the sensing process. The assembled hydrogel sensors can be used for long-term real-time signal monitoring of different human motions. For example, the electrical signals are regularly reproducible at different angles of knee bending (Fig. 12c).

Similarly, highly stretchable MXene composite dual-network hydrogels were synthesized by introducing electrically conductive MXene nanosheets into polyacrylamide (PAM) and sodium alginate (SA) hydrogel networks (Fig. 12e).[156] The high electrical conductivity and sensitivity of hydrogels are attributed to the
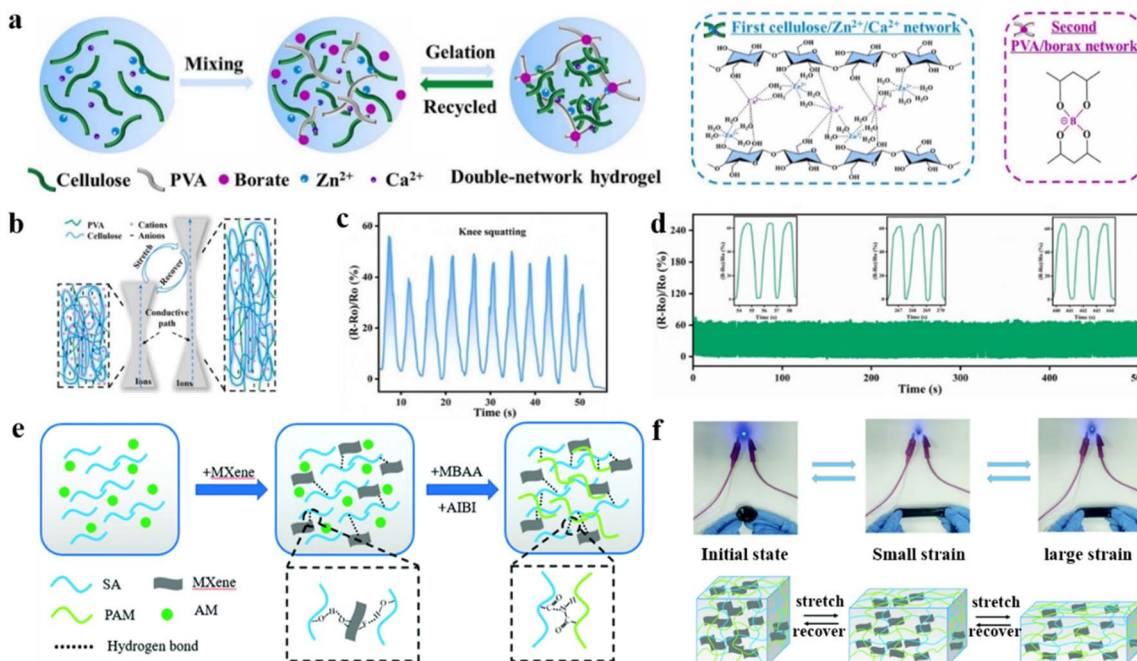
Fig. 12 DN hydrogel modification strategies under extreme mechanical strength conditions. (a) Schematic synthesis of double-network PVA/cellulose hydrogels. (b) Stretching mechanism of hydrogel strain sensors. (c) Relative resistance changes for knee squatting. (d) Relative resistance of the hydrogel strain sensor through 335 continuous cycles of stretching and recovery. Reproduced from ref. 149. Copyright 2024, Elsevier. (e) Schematic illustration of the preparation process of the PAM/SA/MXene hydrogel. (f) Schematic diagram of the PAM/SA/MXene hydrogel during the stretching and release process. Reproduced from ref. 156. Copyright 2022, Royal Society of Chemistry.

formation of a three-dimensional conductive network structure, which is facilitated by the uniform distribution of hydrophilic MXene nanosheets. Meanwhile, the supramolecular interactions between the dual-network matrices improved the mechanical properties of the hydrogels effectively, which resulted in excellent tensile properties (2000%) and tensile cycling stability. In a high mechanical stretching environment, chemical bonds within the brittle network fall victim to energy depletion. The interpenetrating ductile network imparts excellent tensile properties to the hydrogel, which overcomes the lack of tensile properties of single network hydrogels (Fig. 12f).[157] The hydrogel was assembled as a flexible strain sensor, and the GF values are 0.81 and 1.4 when the strain is in the range of 0–100% and 100–2000%, respectively. Moreover, the relative resistance of the hydrogel sensor increased significantly with strain and immediately decreased upon release. This provided fast response (0.75 s) and recovery (0.81 s) performance. The excellent durability of the strain sensor is exhibited by loading and unloading 300 times at 50% tensile strain with the relative resistance value remaining stable. The flexible strain sensors based on double-network structure hydrogels are enabled to monitor the human body movement in real-time, thereby significantly enhancing the potential for these sensing devices in health monitoring applications.

Dual network (DN) hydrogels consisting of (sodium alginate–Zn) SA–Zn and P(AA–AM) (acroleic acid–acrylamide) were prepared by a one-step redox reaction method to improve the mechanical properties, and graphene oxide (GO) was modified by using polydopamine@silver nanoparticles (PDA@Ag) to improve the sensitivity.[158,159] In addition, the construction of the dual network has endowed the hydrogel network with high stretchability for continuous strain sensing. The GO/PDA@Ag/SA–Zn hydrogel strain sensor was prepared with an ultra-low strain detection limit (0.1%), a good gauge factor (GF ∼ 8.29), and high stretchability (600%). Based on the above characteristics, hydrogel strain sensors can be used for continuous monitoring of full-size human body movements, and can be used as a speech interface to recognize the ten types of commonly used words (with 100% accuracy).

4.1.2 Metal ion modification strategies. Stable coordination bonds form due to the coordination interaction between metal ions (Ca^{2+}, Cu^{2+}, Fe^{3+}, etc.) and functional groups (–COOH, –OH, etc.) in the hydrogel network.[160] Compared to hydrogen bonds, metal ion coordination typically exhibits greater binding strength. Hydrogels modified through metal ion coordination have enhanced mechanical strength, while stretching properties are not affected.[161] Meanwhile, the concentration of metal ions significantly affects the conductivity of the hydrogel, thereby enhancing the performance of flexible strain sensors.

Compared to dual network hydrogels, the acid-induced cross-linking of metal ions within the hydrogel network generates sacrificial ionic bonds that possess energy-dissipating capabilities. Additionally, the acid facilitates the uniform release and distribution of calcium ions, which endows the hydrogel with enhanced mechanical tensile properties. Besides,
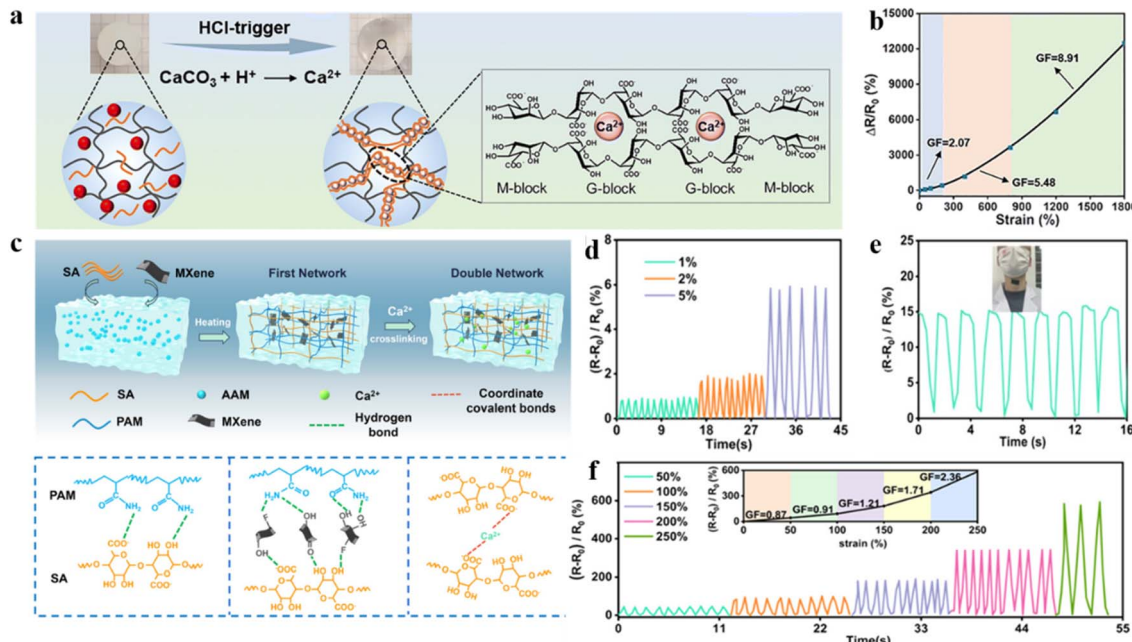
Fig. 13 Metal ion modification strategies under extreme mechanical strength conditions. (a) Schematic diagram of acid-triggered Ca^{2+} release and SA network cross-linking. (b) Relative resistance changes to tensile strain in Ca^{2+}/SA/PAM−DN hydrogels. Reproduced from ref. 162. Copyright 2023, Royal Society of Chemistry. (c) Schematic illustration of the fabrication of the PSM−DN hydrogels. (d) Relative resistance change of the PSM−Ca^{2+} hydrogel based on minor strain. (e) Resistance changes of the PSM−Ca^{2+} hydrogel strain sensor for swallowing movements. (f) Relative resistance change of the PSM−Ca^{2+} hydrogel based on large strain and GF. Reproduced from ref. 163. Copyright 2023, The American Chemical Society.

with optimum calcium ion concentration, larger cross-link density and smaller pores can effectively avoid stress concentration and crack extension. Thus, hydrogels with strong mechanical properties were obtained by introducing Ca^{2+} into sodium alginate/polyacrylamide hydrogels and using acid-induced homogeneous release of calcium ions (Fig. 13a).[162] The utilization of hydrogels for flexible sensors provided a wide strain sensing range (0.03–1800%), fast response time (∼0.02 s), high sensitivity (GF ∼ 8.9), and durability (500 cycles at a strain of 50%) (Fig. 13b). Hydrogel-based flexible strain sensors can be utilized to monitor both human movement and mouse activities.

In order to develop hydrogels with higher sensitivity and excellent mechanical properties, a strategy to improve the mechanical strength of MXene-based dual-network hydrogels through metal ion coordination effects was proposed. In the dual-network hydrogel, MXene nanosheets provide high conductivity, while the strong coordination bonds between metal ions (Ca^{2+}) and sodium alginate (SA) construct the secondary network (Fig. 13c).[163] During the process of stretching, the metal ionic ligand bonds act as energy dissipating sacrificial bonds and the metal–ligand covalent bonds and MXene nanosheets work together to inhibit the inter-sliding between the entangled molecular chains in the hydrogel. Furthermore, the hydrogen-bonded coordination and covalent bonding in the hydrogel network contribute to the molecules recovering to their original state, which significantly improves the durability of the hydrogel. The hydrogel was utilized to

fabricate multifunctional sensors, which demonstrated high sensitivity to minor and major strains. Within small strain ranges, the sensor maintains stable signals even under repeated stretching, thereby enabling precise detection and monitoring of human swallowing movements (Fig. 13d and e). Moreover, the resistance value of hydrogel strain sensors exhibited almost no variation during the continuous tensile cycle test (400 cycles) at 90% strain, which indicated the stability and durability of the sensor (Fig. 13f). Wu and co-authors designed a bilayer-structured polyacrylamide–acrylic acid/Zr^{4+} (P(AAm-co-AAc)/Zr^{4+}) hydrogel with a sandwich pattern made of liquid metal (LM). The moderate water content of the hydrogel matrix is controlled by using carboxyl–Zr^{4+} coordination bonds. It makes the flexible strain sensor highly sensitive and adaptable to high mechanical stretching.[164]

4.1.3 Other modification strategies. The aforementioned modification strategies effectively enhance the strength and toughness of the hydrogel network, thereby significantly widening their application in flexible strain sensors. Furthermore, the mechanical and sensing properties of hydrogel flexible strain sensors can be improved through the construction of semi/interpenetrating networks, nanocomposite hydrogels, and research leveraging the Hofmeister effect, which enable better adaptation to external stimuli and more timely responses.

Conventional hydrogels typically exhibit mono-functionalization and fragile mechanical properties. The semi-interpenetrating network structure of a hydrogel with multiple cross-linking points was constructed by using carboxymethyl
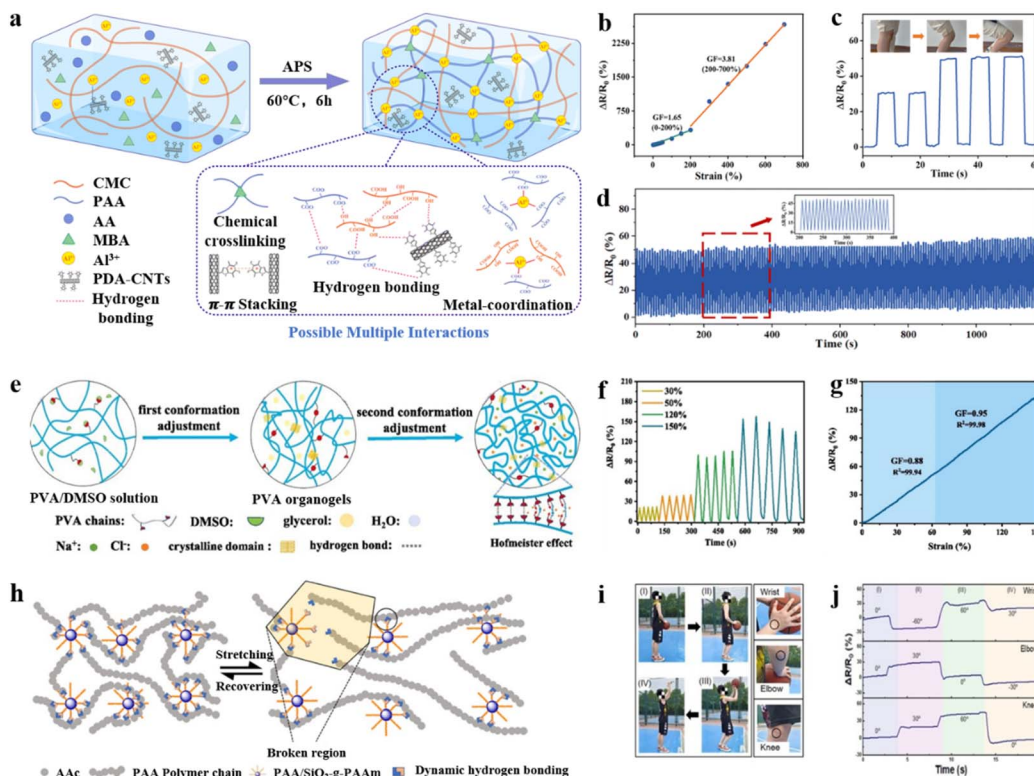
Fig. 14 Other modification strategies under extreme mechanical strength conditions. (a) Schematic illustration of the fabrication of the PDA−CNTs/CMC/PAA hydrogel. (b) Resistance and sensitivity changes of stretch deformation of PDA−CNTs/CMC/PAA hydrogels. (c) Relative resistance changes for knee bending. Reproduced from ref. 165. Copyright 2023, Royal Society of Chemistry. (d) The strain sensor loaded and unloaded for 200 cycles repeatedly at 50% tensile strain. (e) Preparation of PVA hydrogels based on the Hofmeister effect. Relative resistance variation of the hydrogel sensors with (f) tensile strains from 30% to 150%. (g) Gauge factor (GF) of the sensor. Reproduced from ref. 166. Copyright 2024, Elsevier. (h) Schematic diagram of stretching recovery of nanoparticle SiO_2-g-PAAm hydrogels. (i and j) The relative resistance changes of the sensor in different positions during one complete basketball shooting behavior. Reproduced from ref. 170. Copyright 2021, The American Chemical Society.

cellulose (CMC) with rigid chains and polyacrylic acid (PAA) with flexible chains, which conferred the hydrogel with excellent mechanical stretching properties (Fig. 14a).[165] The chemical cross-linking of the polyacrylic acid molecular chain with Al^{3+} leads to metal coordination interaction, which forms multiple cross-linking points. This synergy enhances the conductivity of both electrons and ions, endowing the hydrogel with excellent conductivity (40.1 mS cm^{-1}), sensitivity (GF ∼ 3.81), and mechanical stretchability (Fig. 14b). During the stretching process, the carboxymethylcellulose network with rigid chains may undergo internal fracturing, thereby shielding the polyacrylic acid flexible network from damage by reducing stress concentration. This mechanism provides the hydrogel with remarkable tensile properties (1904%) and toughness (1109.8 kJ m^{-3}). The interaction fatigue test was performed with 200 loading–unloading cycles at 50% strain. After the cycles, $\Delta R/R_0$ remained almost unchanged, demonstrating the excellent stability and durability of the hydrogel sensor (Fig. 14d). In addition, non-covalent interactions such as hydrogen bonding, metal coordination, hydrophobic interactions, and π−π stacking exist between the hydrogel and the object surfaces, ensuring excellent adhesion of the flexible strain sensors under high

mechanical stretching conditions. Based on the above properties, hydrogels used to prepare the strain sensors can be used for real-time monitoring of small muscle changes, information recognition, and transmission. Based on the above characteristics, the strain sensors prepared by using hydrogels can be used not only for real-time monitoring of small changes in muscles, but also for information identification and transmission. Wearable devices for personalized health monitoring and information encryption have a wide range of applications (Fig. 14c).

Compared to biomaterials, achieving a balance between strength and fatigue resistance is challenging due to the relatively low mechanical properties of hydrogels. To address this challenge, mechanically tunable hydrogels with excellent mechanical properties and electrical conductivity were fabricated by synergistically inducing the conformational modification of the molecular chains using solvent exchange and the Hofmeister effect (Fig. 14e).[166] In the hydrogel network, the Hofmeister effect (salting-out effect) can trigger aggregation and rearrangement of PVA chains. In addition, the cooperative action of the salting-out effect through the entanglement of polymer chains induces increased crystallinity, which leads to

the formation of a dense polymer network with a physically cross-linked microcrystalline structure to improve the mechanical stretching properties of hydrogels.[167] The application of hydrogels in flexible strain sensors leads to excellent overall mechanical properties with a superior stretchability of 1252.3 ± 116%, an extraordinarily high strength of 26.4 ± 1.6 MPa, and high sensitivity (GF ∼ 0.95) under 150% strain (Fig. 14f and g). The sensors enable real-time monitoring of human motion (nodding, lifting, bending of the wrist, *etc.*) and can also serve as sensing elements for human–computer interaction.

Nanocomposites are a typical functional material. The formation of hydrogels has the function of physical or chemical cross-linking agent, which endows the hydrogel with excellent mechanical as well as electrical conductivity.[168,169] Under high tensile strain, the nanomaterials efficiently transfer and relieve the loads, which endows the hydrogel with higher fracture strength, elongation, and compressive strain. The core–shell hybridized nanoparticle SiO_2-*g*-PAAM (PAAc (polymer acrylic acid) matrix and the PAAm (polymer acrylamide) chains grafted onto the SiO_2 core were used as physical cross-linking agent centers. The dense dynamic hydrogen bonding between the PAAm ectodomain and the PAAc matrix can enable reversible destruction and reconstruction, de-dissipating large amounts of energy, and can also confer hydrogel flexibility and self-healing properties (Fig. 14h). Due to these unique properties, hydrogels exhibit excellent stretchability (1600%) and self-healing capabilities. The sensors fabricated with the prepared hydrogels exhibited high sensitivity (GF ∼ 5.86) in the strain range of 50% to 500%. Based on the excellent performance, the sensors can be used to monitor a wide range of strains in human movement (*e.g.*, basketball shooting).[170] This research provides a reference

for hydrogel sensors with excellent tensile and sensing properties (Fig. 14i).

4.2 Strong corrosion conditions

Hydrogel flexible strain sensors often fail to maintain structural integrity in strongly corrosive environments, as highly corrosive solvents typically cause swelling of the polymer matrix and weaken the interactions between molecular chains.[171,172] For example, strong acidic solvents can break the hydrogen bonds in hydrogels that rely on physical cross-linking leading to the decomposition of the matrix material.[173] This degradation can erode the conductive network, potentially affecting or altering the electron/ion transport process.[174] Furthermore, the performance of flexible strain sensing is compromised due to increased swelling and loss of mechanical properties in such corrosive environments.[175]

To address this issue, the swelling resistance of hydrogels in strong corrosive solutions was effectively improved by introducing strong chemical bonds and graphene oxide (GO) nanolayers. In addition, the chemical functionalization was effectively promoted by GO surface functional groups, which further improved the corrosion inhibition and mechanical stretching properties of the hydrogel (Fig. 15a).[176–178] The hydrogels were immersed in different polar liquids and exhibited excellent anti-swelling behavior in most solutions (Fig. 15b).[179] Flexible strain sensors prepared from hydrogels maintain structural integrity even after 400 days of immersion in strongly acidic solutions. Remarkably, the sensor even succeeds in enabling accurate and stable sensitivity for tensile strains in a variety of solvents such as water, strongly alkaline solutions, isopropanol, dimethyl sulfoxide, and cyclohexane.
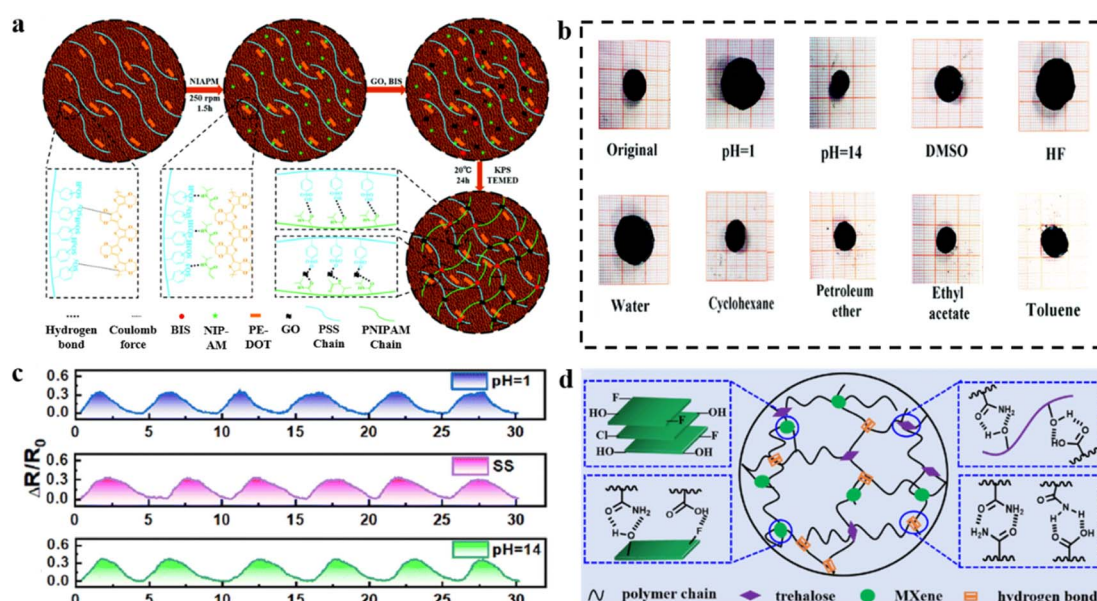

Fig. 15 Modification strategies under strong corrosion conditions. (a) Preparation process of corrosion-resistant hydrogels. (b) Swelling behavior of hydrogels in solutions of different polarities. Reproduced from ref. 179. Copyright 2021, Royal Society of Chemistry. (c) Relative resistance changes of hydrogel strain sensors in solution (pH = 1, pH = 14). (d) Preparation of corrosion-resistant (PMATMx) hydrogels. Reproduced from ref. 180. Copyright 2022, Royal Society of Chemistry.

Nevertheless, hydrogel sensors combine high stretchability (800%), wide sensing range (0.5–800%), fast response time, high sensitivity (GF ∼ 2.17–4.96), and excellent durability (4000 cycles at 30% strain). The sensors can be used directly to detect human motion signals, including joint movements and facial expressions.

Encapsulation is one of the most important strategies to ensure that electronic devices are protected from damage caused by corrosive environments. By incorporating MXenes into the hydrogel network, conductivity is enhanced through their role as a conductive filler, and mechanical properties are improved by increasing the physical cross-linking points within the network.[180] Moreover, the hydrophobic fluorine groups in MXenes modulate the hydrophobicity and increase the bonding strength of the hydrogel to the encapsulation layer (PDMS) (Fig. 15d). Encapsulated hydrogel–elastomer hybrid materials with core–shell structures were developed for use as flexible strain sensors with the advantages of high sensitivity (GF is 2.21, 4.38, and 2.15 in the strain range of 0–60%, 60–120%, and 120–150%, respectively), fast response/recovery (125 ms/140 ms), and stable sensing performance in harsh environments such as acids (pH = 1), alkali (pH = 14), salt solutions (1 M NaCl), and alcohols (Fig. 15c).

5. Summary and outlook

Hydrogels with a unique three-dimensional conductive network have been widely used in the field of flexible strain sensors. However, the applications of hydrogel-based flexible strain sensors under extreme environmental conditions are still in the early stages, with numerous challenges remaining unresolved. In this review, we summarize the main challenges associated with the performance of hydrogel-based flexible strain sensors under various extreme environmental conditions, including extreme temperature, extreme humidity, high mechanical stretching, and high corrosion. Correspondingly, we discuss the improvement strategies proposed to address these challenges in different extreme environments and evaluate their current applications, which remain unsatisfactory. Based on this analysis, we propose the following potential future research directions (Fig. 16):

(1) The depth and prevalence of hydrogel-based strain sensor applications have not yet been thoroughly investigated. Current hydrogel flexible strain sensors are still at the laboratory level and have not been commercialized. The challenges faced in practical applications in various extreme environments are complex. The physical and chemical changes that occur within hydrogel networks in such extreme environments are not well understood and require further exploration, while most research has focused on extreme conditions such as temperature, humidity, and high mechanical stretching; other extreme environments, such as high radiation, also impact hydrogel networks and sensor performance, which needs further investigation. In the future, the application of hydrogel-based flexible strain sensors in various harsh environments can be achieved through material selection and optimization (utilizing high radiation-resistant materials and polymer-based composites with high pressure tolerance), advanced packaging technologies (incorporating metallic materials and composite shielding to ensure sensor integrity), sensor structural design (integrating smart algorithms, self-calibration functions, and compensation mechanisms), and the integration of multiple sensors.

(2) Enhancing the adaptability of strain sensors in extreme environments requires the integration of advanced technologies. The performance of hydrogel flexible strain sensors can be precisely tuned by combining frontier technologies such as 3D
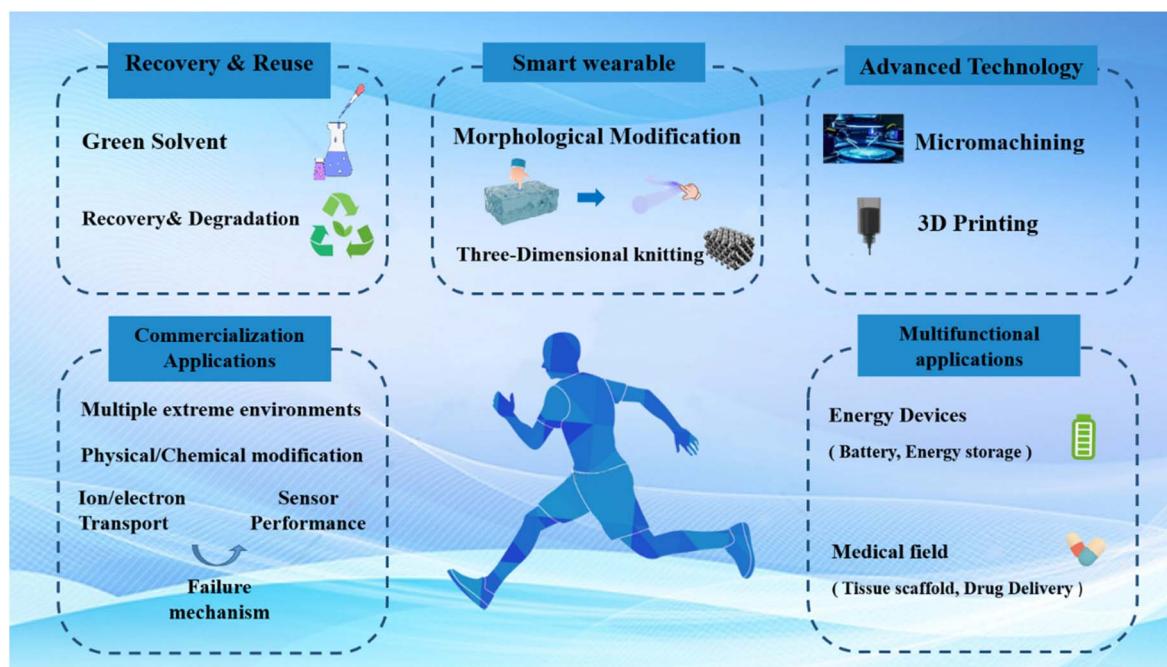
Fig. 16 Proposed future research directions for hydrogel-based flexible strain sensors operating under harsh environmental conditions.

printing and lithography. Additionally, combining these sensors with machine learning and human–computer interaction can enable more efficient and versatile sensing capabilities.

(3) The current form factor of hydrogel-based flexible sensors limits their application in smart wearables. Most existing hydrogel-based flexible sensors are in the form of 2D films or 3D foams, limiting the application of smart wearables. Future research should focus on fabricating fibrous sensors through spinning techniques and integrating them into textiles using weaving technologies such as plain weave and twill weave. This approach would enable sensors to be worn on the body for all-weather, real-time monitoring of physiological conditions.

(4) Exploration of extreme environments not only increases the demand for hydrogel flexible strain sensors but also poses challenges to their reuse and recycling. To enhance the performance of hydrogels in extreme environments, toxic solvents (dimethyl sulfoxide, *etc.*) are often used, which can be hazardous to the human body when used for long periods. In addition, the degrading and recycling of some existing hydrogel materials for flexible strain sensors present significant challenges.

(5) Hydrogels for flexible sensors offer excellent conductivity, enabling integrated applications with other devices. Hydrogels with ionic conductivity not only endow flexible strain sensors with excellent flexibility and sensing properties but also serve as electric and energy storage devices (batteries, nanofriction generators, ionic skin, solar cells, *etc.*). They also have applications in the medical field (drug delivery, tissue engineering scaffolds, *etc.*), *etc.* Therefore, the self-powering of flexible sensors can be realized by integrating sensors and solar cells through conductive hydrogels.

Data availability

No primary research results, software or code have been included and no new data were generated or analysed as part of this review.

Author contributions

M. L. and J. P. engaged in discussions regarding the content and structure. J. P. and Q. C. provided guidance and revisions on the manuscript content. W. Z., Y. G., T. M., and J. C. contributed significant insights. All authors contributed to writing the manuscript. C. G. supervised the whole project.

Conflicts of interest

There are no conflicts to declare.

Acknowledgements

Notes and references

1 S. J. Zheng, X. W. Wang, W. Z. Li, Z. Y. Liu, Q. N. Li and F. Yan, *Nat. Electron.*, 2024, **7**, 576–585.

2 Z. Wang, Y. Liu, Z. Zhou, P. Chen and H. Peng, *Nat. Rev. Electr. Eng.*, 2024, **1**, 466–477.

3 Y. Sun, Y. Su, Z. Chai, L. Jiang and L. Heng, *Nat. Commun.*, 2024, **15**, 7290.

4 L. Zhang, L. Chen, S. Wang, S. Wang, D. Wang, L. Yu, X. Xu, H. Liu and C. Chen, *Nat. Commun.*, 2024, **15**, 3859.

5 A. M. Moran, V. T. Vo, K. J. McDonald, P. Sultania, E. Langenbrunner, J. H. V. Chong, A. Naik, L. Kinnicutt, J. Li and T. Ranzani, *Communications Engineering*, 2024, **3**, 117.

6 Z. Li, Z. Li, W. Tang, J. Yao, Z. Dou, J. Gong, Y. Li, B. Zhang, Y. Dong, J. Xia, L. Sun, P. Jiang, X. Cao, R. Yang, X. Miao and R. Yang, *Nat. Commun.*, 2024, **15**, 7275.

7 B.-H. Xiao, K. Xiao, J.-X. Li, C.-F. Xiao, S. Cao and Z.-Q. Liu, *Chem. Sci.*, 2024, **15**, 11229–11266.

8 S. H. Kim, A. Basir, R. Avila, J. Lim, S. W. Hong, G. Choe, J. H. Shin, J. H. Hwang, S. Y. Park and J. Joo, *Nature*, 2024, **629**, 1047–1054.

9 Z. Ma, W. Shi, K. Yan, L. Pan and G. Yu, *Chem. Sci.*, 2019, **10**, 6232–6244.

10 K. Y. Lee and D. J. Mooney, *Chem. Rev.*, 2001, **101**, 1869–1880.

11 Y. Sun, J. Huang, Y. Cheng, J. Zhang, Y. Shi and L. Pan, *SmartMat*, 2024, e1269.

12 Z. Jiang, N. Chen, Z. Yi, J. Zhong, F. Zhang, S. Ji, R. Liao, Y. Wang, H. Li and Z. Liu, *Nat. Electron.*, 2022, **5**, 784–793.

13 Q. Zhuang, K. Yao, C. Zhang, X. Song, J. Zhou, Y. Zhang, Q. Huang, Y. Zhou, X. Yu and Z. Zheng, *Nat. Electron.*, 2024, **7**, 598–609.

14 Y. Zhang, N. Li, Y. Xiang, D. Wang, P. Zhang, Y. Wang, S. Lu, R. Xu and J. Zhao, *Carbon*, 2020, **156**, 506–513.

15 M. Gwiazda, A. Kaushik, A. Chlanda, E. Kijeńska-Gawrońska, J. Jagiełło, K. Kowiorski, L. Lipińska, W. Święszkowski and S. K. Bhardwaj, *Appl. Surf. Sci. Adv.*, 2022, **9**, 100258.

16 Z. Zhai, X. Zhang, J. Wang, H. Li, Y. Sun, X. Hao, Y. Qin, B. Niu and C. Li, *Chem. Eng. J.*, 2022, **428**, 131720.

17 D. Maurya, S. Khaleghian, R. Sriramdas, P. Kumar, R. A. Kishore, M. G. Kang, V. Kumar, H.-C. Song, S.-Y. Lee and Y. Yan, *Nat. Commun.*, 2020, **11**, 5392.

18 C. Li, S. Cong, Z. Tian, Y. Song, L. Yu, C. Lu, Y. Shao, J. Li, G. Zou and M. H. Rümmeli, *Nano Energy*, 2019, **60**, 247–256.

19 Y. Liu, Z. Xu, X. Ji, X. Xu, F. Chen, X. Pan, Z. Fu, Y. Chen, Z. Zhang and H. Liu, *Nat. Commun.*, 2024, **15**, 5354.

20 S. Seyedin, P. Zhang, M. Naebe, S. Qin, J. Chen, X. Wang and J. M. Razal, *Mater. Horiz.*, 2019, **6**, 219–249.

21 Z. Wang, Y. Cong and J. Fu, *J. Mater. Chem. B*, 2020, **8**, 3437–3459.

22 A. S. Hoffman, *Adv. Drug Delivery Rev.*, 2012, **64**, 18–23.

23 D. Caccavo, S. Cascone, G. Lamberti and A. Barba, *Chem. Soc. Rev.*, 2018, **47**, 2357–2373.

24 J. Zhao, Z. Wang, L. Mo, X. Meng, L. Li and Z. Peng, *Prog. Chem.*, 2022, **34**, 2202.

25 X. Xuan, H. S. Yoon and J. Y. Park, *Biosens. Bioelectron.*, 2018, **109**, 75–82.

26 A. Mehmood, N. Mubarak, M. Khalid, R. Walvekar, E. Abdullah, M. T. H. Siddiqui, H. A. Baloch, S. Nizamuddin and S. Mazari, *J. Environ. Chem. Eng.*, 2020, **8**, 103743.

27 X. Qi, X. Li, H. Jo, K. S. Bhat, S. Kim, J. An, J.-W. Kang and S. Lim, *Sens. Actuators, A*, 2020, **301**, 111697.

28 J. H. Yoon, S.-M. Kim, H. J. Park, Y. K. Kim, D. X. Oh, H.-W. Cho, K. G. Lee, S. Y. Hwang, J. Park and B. G. Choi, *Biosens. Bioelectron.*, 2020, **150**, 111946.

29 J. Pu, Y. Gao, Z. Geng, Y. Zhang, Q. Cao, J. Yang, X. Zhao, Y. Wang, J. Wang and C. Guan, *Adv. Funct. Mater.*, 2024, **34**, 2304453.

30 T. Yan, Y. Wu, J. Tang and Z. Pan, *Mater. Res. Bull.*, 2021, **143**, 111452.

31 Z. Zhao, Q. Li, Y. Dong, J. Gong, Z. Li, X. Qiao and J. Zhang, *Energy Technol.*, 2021, **9**, 2100166.

32 B. Zhang, L. Zhang, W. Deng, L. Jin, F. Chun, H. Pan, B. Gu, H. Zhang, Z. Lv and W. Yang, *ACS Nano*, 2017, **11**, 7440–7446.

33 J. Pu, Y. Gao, Q. Cao, G. Fu, X. Chen, Z. Pan and C. Guan, *SmartMat*, 2022, **3**, 608–618.

34 F. Bu, Y. Gao, W. Zhao, Q. Cao, Y. Deng, J. Chen, J. Pu, J. Yang, Y. Wang and N. Yang, *Angew. Chem.*, 2024, **136**, e202318496.

35 M. Hou, M. Yu, W. Liu, H. Zhang, Z. Wang, J. Du, L. Xu, N. Li and J. Xu, *Chem. Eng. J.*, 2024, **483**, 149299.

36 Q. Zhang, H. Lu, G. Yun, L. Gong, Z. Chen, S. Jin, H. Du, Z. Jiang and W. Li, *Adv. Funct. Mater.*, 2024, **34**, 2308113.

37 Z. Han, P. Wang, Y. Lu, Z. Jia, S. Qu and W. Yang, *Sci. Adv.*, 2022, **8**, eabl5066.

38 Y. Wang, P. Chen, X. Zhou, Y. Liu, N. Wang and C. Gao, *ACS Appl. Mater. Interfaces*, 2022, **14**, 47100–47112.

39 S. Zhang, R. Sun, J. Wang, Z. Jiang, M. Liu, H. Chen, Z. Hu, X. Zhan, F. Gao and Q. Zhang, *Mater. Horiz.*, 2024, DOI: **10.1039/d4mh00970c**.

40 Y. Ni, X. Zang, Y. Yang, Z. Gong, H. Li, J. Chen, C. Wu, J. Huang and Y. Lai, *Adv. Funct. Mater.*, 2024, **34**, 2402853.

41 S. Zhang, F. Guo, X. Gao, M. Yang, X. Huang, D. Zhang, X. Li, Y. Zhang, Y. Shang and A. Cao, *Advanced Science*, 2024, 2405880.

42 S.-N. Li, Z.-R. Yu, B.-F. Guo, K.-Y. Guo, Y. Li, L.-X. Gong, L. Zhao, J. Bae and L.-C. Tang, *Nano Energy*, 2021, **90**, 106502.

43 F. Wang, J. Chen, X. Cui, X. Liu, X. Chang and Y. Zhu, *ACS Appl. Mater. Interfaces*, 2022, **14**, 30268–30278.

44 Q. Feng, K. Wan, C. Zhang and T. Liu, *J. Polym. Sci.*, 2022, **60**, 2710–2719.

45 M. Zhu, X. Wang, H. Tang, J. Wang, Q. Hao, L. Liu, Y. Li, K. Zhang and O. G. Schmidt, *Adv. Funct. Mater.*, 2020, **30**, 1907218.

46 R. Hou, Y. Xie, R. Song, J. Bao, Z. Shi, C. Xiong and Q. Yang, *Cellulose*, 2024, **31**, 4247–4262.

47 Q. Rong, W. Lei, L. Chen, Y. Yin, J. Zhou and M. Liu, *Angew. Chem., Int. Ed.*, 2017, **56**, 14159–14163.

48 L. Li, Y. Zheng, E. Liu, X. Zhao, S. Yu, J Wang, X. Han, F. Xu, Y. Cao and C. Lu, *Chem. Eng. J.*, 2022, **437**, 135399.

49 S. Wu, P. Liu, W. Tong, J. Li, G. Xu, F. Teng, J. Liu, H. Feng, R. Hu and A. Yang, *Compos. Sci. Technol.*, 2023, **231**, 109816.

50 S. Niu, S. He, Y. Chen, Z. Zhu, X. Chang, C. Yang, J. Li, Y. Jiang, D. Wang and Y. Zhu, *Adv. Mater. Technol.*, 2023, **8**, 2300867.

51 L. Zhao, Q. Ling, X. Fan and H. Gu, *ACS Appl. Mater. Interfaces*, 2023, **15**, 40975–40990.

52 J. S. Kim and A. Yethiraj, *J. Chem. Phys.*, 2008, **129**, 124504.

53 B. Yao, S. Wu, R. Wang, Y. Yan, A. Cardenas, D. Wu, Y. Alsaid, W. Wu, X. Zhu and X. He, *Adv. Funct. Mater.*, 2022, **32**, 2109506.

54 Z. Liu, J. Zhang, J. Liu, Y. Long, L. Fang, Q. Wang and T. Liu, *J. Mater. Chem. A*, 2020, **8**, 6219–6228.

55 Y. Wang, L. Zhang and A. Lu, *ACS Appl. Mater. Interfaces*, 2019, **11**, 41710–41716.

56 H. Liu, X. Wang, Y. Cao, Y. Yang, Y. Yang, Y. Gao, Z. Ma, J. Wang, W. Wang and D. Wu, *ACS Appl. Mater. Interfaces*, 2020, **12**, 25334–25344.

57 C. Luo, X. Deng and S. Xie, *J. Mater. Chem. C*, 2021, **9**, 17042–17049.

58 O. Morgenstern, F. M. O'Connor, B. T. Johnson, G. Zeng, J. P. Mulcahy, J. Williams, J. Teixeira, M. Michou, P. Nabat, L. W. Horowitz, V. Naik, L. T. Sentman, M. Deushi, S. E. Bauer, K. Tsigaridis, D. T. Shindell and D. E. Kinnison, *Geophys. Res. Lett.*, 2020, **47**, e2020GL088295.

59 Z. Wu, G. Guo, B. K. Biswal, J. Dai and G. Chen, *Bioresour. Technol.*, 2020, **313**, 123574.

60 W. Wang, S. Xu, Q. Li and S. Dong, *Constr. Build. Mater.*, 2022, **317**, 126164.

61 C. Wang, B. Yang, R. Xiang, J. Ji, Y. Wu and S. Tan, *ACS Nano*, 2023, **17**, 23194–23206.

62 S.-N. Li, X.-F. He, Z.-F. Zeng, B. Jiang, Q. Wu, L.-X. Gong, Y. Li, J. Bae, S. Wang and L.-C. Tang, *Nano Energy*, 2022, **103**, 107789.

63 G. Chen, J. Huang, J. Gu, S. Peng, X. Xiang, K. Chen, X. Yang, L. Guan, X. Jiang and L. Hou, *J. Mater. Chem. A*, 2020, **8**, 6776–6784.

64 Z. He, Z. Zhou and W. Yuan, *ACS Appl. Mater. Interfaces*, 2022, **14**, 38205–38215.

65 Z. Wu, W. Shi, H. Ding, B. Zhong, W. Huang, Y. Zhou, X. Gui, X. Xie and J. Wu, *J. Mater. Chem. C*, 2021, **9**, 13668–13679.

66 A. Chandra, *Phys. Rev. Lett.*, 2000, **85**, 768.

67 H. Liao, X. Guo, P. Wan and G. Yu, *Adv. Funct. Mater.*, 2019, **29**, 1904507.

68 Y. Zhao, Z. Chen, F. Mo, D. Wang, Y. Guo, Z. Liu, X. Li, Q. Li, G. Liang and C. Zhi, *Advanced Science*, 2021, **8**, 2002590.

69 L.-Y. Zeng, X.-C. Wang, Y. Wen, H.-M. Chen, H.-L. Ni, W.-H. Yu, Y.-F. Bai, K.-Q. Zhao and P. Hu, *Carbohydr. Polym.*, 2023, **300**, 120229.

70 Z. Qin, D. Dong, M. Yao, Q. Yu, X. Sun, Q. Guo, H. Zhang, F. Yao and J. Li, *ACS Appl. Mater. Interfaces*, 2019, **11**, 21184–21193.

71 X. Pan, Q. Wang, R. Guo, Y. Ni, K. Liu, X. Ouyang, L. Chen, L. Huang, S. Cao and M. Xie, *J. Mater. Chem. A*, 2019, **7**, 4525–4535.

72 S. Bao, J. Gao, T. Xu, N. Li, W. Chen and W. Lu, *Chem. Eng. J.*, 2021, **411**, 128470.

73 Y. Jian, S. Handschuh-Wang, J. Zhang, W. Lu, X. Zhou and T. Chen, *Mater. Horiz.*, 2021, **8**, 351–369.

74 D. Sun, N. Li, J. Rao, S. Jia, Z. Su, X. Hao and F. Peng, *J. Mater. Chem. A*, 2021, **9**, 14381–14391.

75 C. Shao, M. Wang, L. Meng, H. Chang, B. Wang, F. Xu, J. Yang and P. Wan, *Chem. Mater.*, 2018, **30**, 3110–3121.

76 J. Cai, X. Zhang, W. Liu, J. Huang and X. Qiu, *Polymer*, 2020, **202**, 122643.

77 Y. Liu, G. Tian, Y. Du, P. Shi, N. Li, Y. Li, Z. Qin, T. Jiao and X. He, *Adv. Funct. Mater.*, 2024, **34**, 2315813.

78 J. Zhang, Y. Liang, Z. Deng, H. Xu, H. Zhang, B. Guo and J. Zhang, *ACS Appl. Mater. Interfaces*, 2023, **15**, 29902–29913.

79 L. Xu, Z. Huang, Z. Deng, Z. Du, T. L. Sun, Z. H. Guo and K. Yue, *Adv. Mater.*, 2021, **33**, 2105306.

80 A. Agafonov, L. Ramenskaya, E. Grishina and N. Kudryakova, *RSC Adv.*, 2021, **11**, 38605–38615.

81 Q. Xu, M. Hou, L. Wang, X. Zhang and L. Liu, *Chem. Eng. J.*, 2023, **477**, 147065.

82 W. Zhao, J. Jiang, W. Chen, Y. He, T. Lin and L. Zhao, *Chem. Eng. J.*, 2023, **468**, 143660.

83 D. M. Correia, L. C. Fernandes, M. M. Fernandes, B. Hermenegildo, R. M. Meira, C. Ribeiro, S. Ribeiro, J. Reguera and S. Lanceros-Mendez, *Nanomaterials*, 2021, **11**, 2401.

84 J. Liu, X. Zhang, Y. Cui, Y. Liu, W. Wang, Y. Guo, Q. Wang and X. Dong, *ACS Appl. Mater. Interfaces*, 2024, **16**, 5208–5216.

85 Y. Ye, H. Oguzlu, J. Zhu, P. Zhu, P. Yang, Y. Zhu, Z. Wan, O. J. Rojas and F. Jiang, *Adv. Funct. Mater.*, 2023, **33**, 2209787.

86 R. Liu, L. Cui, H. Wang, Q. Chen, Y. Guan and Y. Zhang, *Results Phys.*, 2021, **13**(35), 42052–42062.

87 Y. Yang, Y. Yang, Y. Cao, X. Wang, Y. Chen, H. Liu, Y. Gao, J. Wang, C. Liu and W. Wang, *Chem. Eng. J.*, 2021, **403**, 126431.

88 Y. Wang, Y. Xia, P. Xiang, Y. Dai, Y. Gao, H. Xu, J. Yu, G. Gao and K. Chen, *Chem. Eng. J.*, 2022, **428**, 131171.

89 Z. He, C. Wu, M. Hua, S. Wu, D. Wu, X. Zhu, J. Wang and X. He, *Matter*, 2020, **2**, 723–734.

90 I. K. Voets, *Soft Matter*, 2017, **13**, 4808–4823.

91 R. Liu, Y. Liu, S. Fu, Y. Cheng, K. Jin, J. Ma, Y. Wan and Y. Tian, *Small*, 2024, **20**, 2308092.

92 D. Sun, Y. Feng, S. Sun, J. Yu, S. Jia, C. Dang, X. Hao, J. Yang, W. Ren, R. Sun, C. Shao and F. Peng, *Adv. Funct. Mater.*, 2022, **32**, 2201335.

93 Y. K. Choi, T. Park, D. H. D. Lee, J. Ahn, Y. H. Kim, S. Jeon, M. J. Han and S. J. Oh, *Nanoscale*, 2022, **14**, 8628–8639.

94 T. Park, H. K. Woo, B. K. Jung, B. Park, J. Bang, W. Kim, S. Jeon, J. Ahn, Y. Lee and Y. M. Lee, *ACS Nano*, 2021, **15**, 8120–8129.

95 W. Xu, T. Shen, Y. Ding, H. Ye, B. Wu and F. Chen, *Small*, 2024, **20**, 2310072.

96 G. Su, Y. Zhang, X. Zhang, J. Feng, J. Cao, X. Zhang and T. Zhou, *Chem. Mater.*, 2022, **34**, 1392–1402.

97 H. Sun, Y. Zhao, S. Jiao, C. Wang, Y. Jia, K. Dai, G. Zheng, C. Liu, P. Wan and C. Shen, *Adv. Funct. Mater.*, 2021, **31**, 2101696.

98 M. Li, Y. Yang, C. Yue, Y. Song, M. Manzo, Z. Huang and L. Cai, *Cellulose*, 2022, **29**, 1897–1909.

99 L. Zhou, B. Zhao, J. Liang, F. Lu, W. Yang, J. Xu, J. Zheng, Y. Liu, R. Wang and Z. Liu, *Mater. Horiz.*, 2024, **11**, 3856–3866.

100 Y. Bai, B. Chen, F. Xiang, J. Zhou, H. Wang and Z. Suo, *Appl. Phys. Lett.*, 2014, **105**, 151903.

101 C. Cai, C. Wen, W. Zhao, S. Tian, Y. Long, X. Zhang, X. Sui, L. Zhang and J. Yang, *ACS Appl. Mater. Interfaces*, 2022, **14**, 23692–23700.

102 H. Zhou, J. Lai, X. Jin, H. Liu, X. Li, W. Chen, A. Ma and X. Zhou, *Chem. Eng. J.*, 2021, **413**, 127544.

103 S. Shi, X. Peng, T. Liu, Y.-N. Chen, C. He and H. Wang, *Polymer*, 2017, **111**, 168–176.

104 L. Han, K. Liu, M. Wang, K. Wang, L. Fang, H. Chen, J. Zhou and X. Lu, *Adv. Funct. Mater.*, 2018, **28**, 1704195.

105 Y. Lu, Y. Yue, Q. Ding, C. Mei, X. Xu, S. Jiang, S. He, Q. Wu, H. Xiao and J. Han, *Infomat*, 2023, **5**, e12409.

106 T. Zhu, C. Jiang, M. Wang, C. Zhu, N. Zhao and J. Xu, *Adv. Funct. Mater.*, 2021, **31**, 2102433.

107 H. Chen, J. Huang, J. Liu, J. Gu, J. Zhu, B. Huang, J. Bai, J. Guo, X. Yang and L. Guan, *J. Mater. Chem. A*, 2021, **9**, 23243–23255.

108 B. Li, J. Luo, X. Huang, L. Lin, L. Wang, M. Hu, L. Tang, H. Xue, J. Gao and Y.-W. Mai, *Composites, Part B*, 2020, **181**, 107580.

109 J. Wu, W. Huang, Z. Wu, X. Yang, A. G. P. Kottapalli, X. Xie, Y. Zhou and K. Tao, *ACS Mater. Lett.*, 2022, **4**, 1616–1629.

110 Q. Wang, X. Zhou, J. Zeng and J. Wang, *Nucl. Instrum. Methods Phys. Res., Sect. B*, 2016, **368**, 90–95.

111 Z. Chen, Y. Li and Q. M. Li, *Mater. Des.*, 2021, **207**, 109819.

112 S. Mousazadeh and M. Kokabi, *Polymer*, 2020, **191**, 122280.

113 Y. Zhan, W. Fu, Y. Xing, X. Ma and C. Chen, *Mater. Sci. Eng., C*, 2021, **127**, 112208.

114 D. Yao, L. Wu, S. Peng, X. Gao, C. Lu, Z. Yu, X. Wang, C. Li and Y. He, *ACS Appl. Mater. Interfaces*, 2021, **13**, 11284–11295.

115 H. Omidian and K. Park, *Biomedical applications of hydrogels handbook*, 2010, vol. 1, pp. 1–16.

116 Y. Cai, K. Wan, Q. Chen, M. Hong, Z.-X. Zhou and H. Fu, *J. Mater. Chem. C*, 2023, **11**, 12981–12991.

117 C. Qi, Z. Dong, Y. Huang, J. Xu and C. Lei, *ACS Appl. Mater. Interfaces*, 2022, **14**, 30385–30397.

118 M. Antonietti, J. Conrad and A. Thuenemann, *Macromolecules*, 1994, **27**, 6007–6011.

119 P. Du, J. Wang, Y.-I. Hsu and H. Uyama, *Chem. Mater.*, 2024, **36**, 1318–1332.

120 S. Wang, L. Wang, X. Qu, B. Lei, Y. Zhao, Q. Wang, W. Wang, J. Shao and X. Dong, *ACS Appl. Mater. Interfaces*, 2022, **14**, 50256–50265.

121 J. Wei, Y. Zheng and T. Chen, *Mater. Horiz.*, 2021, **8**, 2761–2770.

122 Z. Sun, C. Dong, B. Chen, W. Li, H. Hu, J. Zhou, C. Li and Z. Huang, *Small*, 2023, **19**, 2303612.

123 J. Ren, Y. Liu, Z. Wang, S. Chen, Y. Ma, H. Wei and S. Lü, *Adv. Funct. Mater.*, 2022, **32**, 2107404.

124 Z. Wang, S. Lü, Y. Liu, T. Li, J. Yan, X. Bai, B. Ni, J. Yang and M. Liu, *ACS Appl. Mater. Interfaces*, 2019, **11**, 31393–31401.

125 X. Hu, S. Chen, H. Wang, Z.-X. Zhou, J. Min, Q. Chen, M. Hong and H. Fu, *React. Funct. Polym.*, 2023, **190**, 105624.

126 J. Wu, Z. Wu, X. Lu, S. Han, B.-R. Yang, X. Gui, K. Tao, J. Miao and C. Liu, *ACS Appl. Mater. Interfaces*, 2019, **11**, 9405–9414.

127 Y. Chen, Y. Xu, Q. Gao, H. Qian and R. Yang, *IEEE Sens. J.*, 2020, **21**, 6802–6810.

128 X. Li, D. Lou, H. Wang, X. Sun, J. Li and Y. N. Liu, *Adv. Funct. Mater.*, 2020, **30**, 2007291.

129 L. Zhao, H. Xu, L. Liu, Y. Zheng, W. Han and L. Wang, *Advanced Science*, 2023, **10**, 2303922.

130 L. Han, X. Lu, M. Wang, D. Gan, W. Deng, K. Wang, L. Fang, K. Liu, C. W. Chan and Y. Tang, *Small*, 2017, **13**, 1601916.

131 J. Huang, R. Zhou, Z. Chen, Y. Wang, Z. Li, X. Mo, N. Gao, J. He and C. Pan, *Mater. Today Phys.*, 2023, **35**, 101123.

132 C. Wang, Y. Liu, X. Qu, B. Shi, Q. Zheng, X. Lin, S. Chao, C. Wang, J. Zhou and Y. Sun, *Adv. Mater.*, 2022, **34**, 2105416.

133 X. Sui, H. Guo, C. Cai, Q. Li, C. Wen, X. Zhang, X. Wang, J. Yang and L. Zhang, *Chem. Eng. J.*, 2021, **419**, 129478.

134 M. Guo, J. Yan, X. Yang, J. Lai, P. An, Y. Wu, Z. Li, W. Lei, A. T. Smith and L. Sun, *J. Mater. Chem. A*, 2021, **9**, 7935–7945.

135 J. Wen, J. Tang, H. Ning, N. Hu, Y. Zhu, Y. Gong, C. Xu, Q. Zhao, X. Jiang, X. Hu, L. Lei, D. Wu and T. Huang, *Adv. Funct. Mater.*, 2021, **31**, 2011176.

136 S. Zhao, Y. Zuo, T. Liu, S. Zhai, Y. Dai, Z. Guo, Y. Wang, Q. He, L. Xia, C. Zhi, J. Bae, K. Wang and M. Ni, *Adv. Energy Mater.*, 2021, **11**, 2101749.

137 W. Wang, X. Deng, J. Lu and C. Luo, *J. Mater. Chem. C*, 2023, **11**, 13857–13864.

138 M. T. I. Mredha, H. H. Le, J. Cui and I. Jeon, *Advanced Science*, 2020, **7**, 1903145.

139 H. Zhu, J. Xu, X. Sun, Q. Guo, Q. Guo, M. Jiang, K. Wu, R. Cai and K. Qian, *J. Mater. Chem. A*, 2022, **10**, 23366–23374.

140 J. Yang, J. Cheng, G. Qi and B. Wang, *ACS Appl. Mater. Interfaces*, 2023, **15**, 17163–17174.

141 X. Meng, Y. Qiao, C. Do, W. Bras, C. He, Y. Ke, T. P. Russell and D. Qiu, *Adv. Mater.*, 2022, **34**, 2108243.

142 X. Meng, Y. Qiao, C. Do, W. Bras, C. He, Y. Ke, T. P. Russell and D. Qiu, *Adv. Mater.*, 2022, **34**, 2108243.

143 H. Yao, W. Yang, W. Cheng, Y. J. Tan, H. H. See, S. Li, H. P. A. Ali, B. Z. Lim, Z. Liu and B. C. Tee, *Proc. Natl. Acad. Sci. U. S. A.*, 2020, **117**, 25352–25359.

144 X. Liu, J. Miao, Q. Fan, W. Zhang, X. Zuo, M. Tian, S. Zhu, X. Zhang and L. Qu, *Adv. Fiber Mater.*, 2022, **4**, 361–389.

145 H. Liu, C. Liu, J. Luo, H. Tang, Y. Li, H. Liu, J. Wu, F. Han, Z. Liu and J. Guo, *InfoMat*, 2024, **6**, e12511.

146 H. Zhang, W. Niu and S. Zhang, *ACS Appl. Mater. Interfaces*, 2018, **10**, 32640–32648.

147 J. P. Gong, Y. Katsuyama, T. Kurokawa and Y. Osada, *Adv. Mater.*, 2003, **15**, 1155–1158.

148 K. Lei, M. Chen, P. Guo, J. Fang, J. Zhang, X. Liu, W. Wang, Y. Li, Z. Hu, Y. Ma, H. Jiang, J. Cui and J. Li, *Adv. Funct. Mater.*, 2023, **33**, 2303511.

149 Y. Wang, Y. Zhang, P. Ren, S. Yu, P. Cui, C. B. Nielsen, I. Abrahams, J. Briscoe and Y. Lu, *Nano Energy*, 2024, **125**, 109599.

150 J. Han, T. Lei and Q. Wu, *Carbohydr. Polym.*, 2014, **102**, 306–316.

151 J.-n. Liu, Q. He, M.-y. Pan, K. Du, C.-B. Gong and Q. Tang, *J. Mater. Chem. A*, 2022, **10**, 25118–25128.

152 M. Liao, P. Wan, J. Wen, M. Gong, X. Wu, Y. Wang, R. Shi and L. Zhang, *Adv. Funct. Mater.*, 2017, **27**, 1703852.

153 Q. Chen, H. Chen, L. Zhu and J. Zheng, *J. Mater. Chem. B*, 2015, **3**, 3654–3676.

154 Y. Zhou, C. Wan, Y. Yang, H. Yang, S. Wang, Z. Dai, K. Ji, H. Jiang, X. Chen and Y. Long, *Adv. Funct. Mater.*, 2019, **29**, 1806220.

155 H. Zheng, N. Lin, Y. He and B. Zuo, *ACS Appl. Mater. Interfaces*, 2021, **13**, 40013–40031.

156 H. Luan, D. Zhang, Z. Xu, W. Zhao, C. Yang and X. Chen, *J. Mater. Chem. C*, 2022, **10**, 7604–7613.

157 S. Han, C. Liu, X. Lin, J. Zheng, J. Wu and C. Liu, *ACS Appl. Polym. Mater.*, 2020, **2**, 996–1005.

158 J. Zhou, T. Chen, Z. He, L. Sheng and X. Lu, *J. Mater. Chem. C*, 2023, **11**, 13476–13487.

159 W. Feng, H. Luo, Y. Wang, S. Zeng, L. Deng, X. Zhou, H. Zhang and S. Peng, *RSC Adv.*, 2018, **8**, 2398–2403.

160 Y. Huang, L. Xiao, J. Zhou, T. Liu, Y. Yan, S. Long and X. Li, *Adv. Funct. Mater.*, 2021, **31**, 2103917.

161 T. Long, Y. Li, X. Fang and J. Sun, *Adv. Funct. Mater.*, 2018, **28**, 1804416.

162 X. Zhang, H. Geng, X. Zhang, Y. Liu, J. Hao and J. Cui, *J. Mater. Chem. A*, 2023, **11**, 2996–3007.

163 Q. Yang, M. Li, R. Chen, D. Gao, Z. Wang, C. Qin, W. Yang, H. Liu and P. Zhang, *ACS Appl. Mater. Interfaces*, 2023, **15**, 51774–51784.

164 H. Wu, H. Qi, X. Wang, Y. Qiu, K. Shi, H. Zhang, Z. Zhang, W. Zhang and Y. Tian, *J. Mater. Chem. C*, 2022, **10**, 8206–8217.

165 L. Xing, Y. Song, X. Zou, H. Tan, J. Yan and J. Wang, *J. Mater. Chem. C*, 2023, **11**, 13376–13386.

166 H. Wu, Y. Wu, J. Yan, W. Xiao, Y. Wang, H. Zhang, X. Huang, H. Xue, L. Wang, L. Tang, Y. Mai and J. Gao, *Chem. Eng. J.*, 2024, **488**, 150963.

167 J. Kim, G. Zhang, M. Shi and Z. Suo, *Science*, 2021, **374**, 212–216.

168 A. Motealleh and N. S. Kehr, *Adv. Healthcare Mater.*, 2017, **6**, 1600938.

169 D. Gan, T. Shuai, X. Wang, Z. Huang, F. Ren, L. Fang, K. Wang, C. Xie and X. Lu, *Nano-Micro Lett.*, 2020, **12**, 1–16.

170 X. Yu, Y. Zheng, H. Zhang, Y. Wang, X. Fan and T. Liu, *Chem. Mater.*, 2021, **33**, 6146–6157.

171 X. Liu, Q. Zhang, L. Duan and G. Gao, *Adv. Funct. Mater.*, 2019, **29**, 1900450.

172 P. Rao, T. L. Sun, L. Chen, R. Takahashi, G. Shinohara, H. Guo, D. R. King, T. Kurokawa and J. P. Gong, *Adv. Mater.*, 2018, **30**, 1801884.

173 K. Haraguchi, Y. Xu and G. Li, *Macromol. Rapid Commun.*, 2010, **31**, 718–723.

174 J. Yin, W. Sun, X. Song, H. Ji, Y. Yang, S. Sun, W. Zhao and C. Zhao, *Sep. Purif. Technol.*, 2020, **238**, 116497.

175 J. Ma, Z. Li, H. Song, X. Xu, C. Long, Y. Li, Y. Qing and C. Liu, *Chem. Eng. J.*, 2024, **488**, 150797.

176 H. Gotoh, C. Liu, A. B. Imran, M. Hara, T. Seki, K. Mayumi, K. Ito and Y. Takeoka, *Sci. Adv.*, 2018, **4**, eaat7629.

177 J. Liu, J. Huang, Q. Cai, Y. Yang, W. Luo, B. Zeng, Y. Xu, C. Yuan and L. Dai, *ACS Appl. Mater. Interfaces*, 2020, **12**, 20479–20489.

178 O. Galant, S. Bae, M. N. Silberstein and C. E. Diesendruck, *Adv. Funct. Mater.*, 2020, **30**, 1901806.

179 H. Zhang, M. Yue, T. Wang, J. Wang, X. Wu and S. Yang, *New J. Chem.*, 2021, **45**, 4647–4657.

180 S. Dai, H. Hu, Y. Zhang, J. Xu, Y. Zhong, G. Cheng and J. Ding, *J. Mater. Chem. C*, 2023, **11**, 2688–2694.